Atmos. Chem. Phys. Discuss., https://doi.org/10.5194/acp-2019-254
Manuscript under review for journal Atmos. Chem. Phys.
Discussion started: 29 March 2019

Atmospheric Chemistry and Physics Discussions

Controls on the water vapor isotopic composition near the surface of tropical oceans and role of boundary layer mixing processes

Camille Risi[1], Joseph Galewsky[2], Gilles Reverdin[3], and Florent Brient[4]

[1]Laboratoire de Météorologie Dynamique, IPSL, CNRS, Sorbonne Université, Paris, France
[2]Department of Earth and Planetary Sciences, University of New Mexico, Albuquerque, USA
[3]LOCEAN, IPSL, CNRS, Sorbonne Université, Paris, France
[4]CNRM, Université de Toulouse, Météo-France, CNRS, Toulouse, France

Correspondence: Camille Risi (Camille.Risi@lmd.jussieu.fr)

Abstract. Understanding what controls the water vapor isotopic composition of the sub-cloud layer (SCL) over tropical oceans (δD_0) is a first step towards understanding the water vapor isotopic composition everywhere in the troposphere. We propose an analytical model to predict δD_0 as a function of sea surface conditions, humidity and temperature profiles, and the altitude from which the free tropospheric air originates (z_{orig}). To do so, we extend previous studies by (1) prescribing the shape of δD vertical profiles, and (2) linking δD_0 to z_{orig}. The model relies on the hypotheses that δD profiles are steeper than mixing lines and no clouds are precipitating. We show that δD_0 does not depend on the intensity of entrainment, dampening hope that δD_0 measurements could help constrain this long-searched quantity. Based on an isotope-enabled general circulation model simulation, we show that δD_0 variations are mainly controlled by mid-tropospheric depletion and rain evaporation in ascending regions, and by sea surface temperature and z_{orig} in subsiding regions. When the air mixing into the SCL is lower in altitude, it is moister, and thus it depletes more efficiently the SCL. In turn, could δD_0 measurements help estimate z_{orig} and thus discriminate between different mixing processes? Estimates that are accurate enough to be useful would be difficult to achieve in practice, requiring measuring daily δD profiles, and measuring δD_0 with an accuracy of 0.1 ‰ and 0.4 ‰ in trade-wind cumulus and strato-cumulus clouds respectively.

1 Introduction

1.1 What controls the water vapor isotopic composition?

The water vapor isotopic composition (e.g. $\delta D = (R/R_{SMOW} - 1) \times 1000$ expressed in ‰, where $R = HDO/H_2O$ and SMOW is the Standard Mean Ocean Water reference) has been shown to be sensitive to a wide range of atmospheric processes (Galewsky et al., 2016), such as continental recycling (Salati et al., 1979; Risi et al., 2013), unsaturated downdrafts (Risi et al., 2008, 2010a), rain evaporation (Worden et al., 2007; Field et al., 2010), the degree of organization of convection

Atmos. Chem. Phys. Discuss., https://doi.org/10.5194/acp-2019-254
Manuscript under review for journal Atmos. Chem. Phys.
Discussion started: 29 March 2019

Atmospheric Chemistry and Physics Discussions

(Lawrence et al., 2004; Tremoy et al., 2014), the convective depth (Lacour et al., 2017), the proportion of precipitation that occurs as convective or large-scale precipitation (Lee et al., 2009; Kurita, 2013; Aggarwal et al., 2016), vertical mixing in the lower troposphere (Benetti et al., 2015; Galewsky, 2018a, b), mid-troposphere (Risi et al., 2012b) or upper-troposphere (Galewsky and Samuels-Crow, 2014), convective detrainment (Moyer et al., 1996; Webster and Heymsfield, 2003), ice microphysics (Bolot et al., 2013). It is therefore very challenging to quantitatively understand what controls the isotopic composition of water vapor.

A first step towards this goal is to understand what controls the water vapor isotopic composition in the sub-cloud layer (SCL) of tropical (30°S-30°N) oceans. Indeed, this water vapor is a important source moistening air masses traveling to land regions (Gimeno et al., 2010; Ent and Savenije, 2013) and towards higher latitudes (Ciais et al., 1995; Delaygue et al., 2000). It is also ultimately the only source of water vapor in the tropical free troposphere, since water vapor in the free troposphere ultimately originates from convective detrainment (Sherwood, 1996), and convection ultimately feeds from the SCL air (Bony et al., 2008). Therefore, the water vapor isotopic composition in the SCL of tropical oceans serves as initial conditions to understand the isotopic composition in land waters and in the tropospheric water vapor everywhere on Earth. We focus here on the SCL because, by definition, there is no complication by cloud condensation processes.

The goal of this paper is thus to propose a simple analytical equation that allows us to understand and quantify the factors controlling the δD in the water vapor in the SCL of tropical oceans. So far, the most famous analytical equation for this purpose has been the closure equation developed by Merlivat and Jouzel (1979) (MJ79). This closure equation can be derived by assuming that all the water vapor in the SCL air originates from surface evaporation. The water balance of the SCL can be closed by assuming a mass export at the SCL top (e.g. by convective mass fluxes) and a totally dry entrainment into the SCL to compensate this mass export. The MJ79 equation has proved very useful to capture the sensitivity of δD and second-order parameter d-excess to sea-surface conditions (Merlivat and Jouzel, 1979; Ciais et al., 1995; Risi et al., 2010d). However, the δD calculated from this equation suffers a low bias in tropical regions (Jouzel and Koster, 1996). This bias can be explained by the neglect of vertical mixing between the SCL and air entrained from the free troposphere (FT). The MJ79 equation can better reproduce surface water vapor observation when extended to take into account this mixing (Benetti et al., 2015), hereafter B15). However, this extension requires to know the specific humidity (q) and water vapor δD of the entrained air, which are often unknown. In addition, they assumed that the air entrained into the boundary layer comes from a constant altitude, which does not reflects the complexity of entrainment and mixing processes in marine boundary layers.

1.2 Entrainment and mixing mechanisms

Figure 1 summarizes our knowledge about these entrainment and mixing processes. In strato-cumulus regions, clouds are thin and the inversion is just above the LCL. Air is entrained from the FT by cloud-top entrainment driven by radiative cooling or wind shear instabilities (Mellado, 2017), possibly amplified by evaporative cooling of droplets (Lozar and Mellado, 2015). Both Direct Numerical Simulations (Mellado, 2017) and observations of tracers (Faloona et al., 2005) and cloud holes (Gerber et al., 2005) show that air is entrained from a thin layer above the inversion, thinner than 80m and as small as 5m. The boundary

Atmos. Chem. Phys. Discuss., https://doi.org/10.5194/acp-2019-254
Manuscript under review for journal Atmos. Chem. Phys.
Discussion started: 29 March 2019

Atmospheric Chemistry and Physics Discussions

layer itself is animated by updrafts, downdrafts and associated turbulent shells that bring air from the cloud layer downward (Brient et al., 2019; Davini et al., 2017).

In trade-wind cumulus regions, the cloudy layer is a bit deeper. Observational studies and large-eddy simulations have pointed the important role of thin subsiding shells around cumulus clouds, driven by mixing and evaporative cooling of droplets (Jonas, 1990; Rodts et al., 2003; Heus and Jonker, 2008; Heus et al., 2009; Park et al., 2016). This brings air from the cloudy layer to the SCL. Subsiding shells may also cover overshooting plumes of the cumulus clouds, entraining FT air into the cloud layer (Heus and Jonker, 2008).

In deep convective regions, unsaturated downdrafts driven by rain evaporation (Zipser, 1977) are known to contribute significantly to the energy budget of the SCL (Emanuel et al., 1994). Large-eddy simulations show that subsiding shells, similar to those documented in shallow convection, also exist around deep convective clouds (Glenn and Krueger, 2014). In the clear-sky environment between clouds, turbulent entrainment into the SCL may also play a significant role (Thayer-Calder and Randall, 2015).

Therefore, whatever the cloud regime, air entering the SCL from above may originate either from the cloud layer or from the free troposphere, depending on the mixing mechanism. Therefore, in this paper in contrast with Benetti et al. (2015), we let the altitude from which the air originates, z_{orig}, be variable. We do not call it "entrained" air because entrainment sometimes refer to mixing processes through an interface (e.g. De Rooy et al. (2013); Davini et al. (2017)), whereas air in the SCL may also enter through deep, coherent and penetrative structures such as unsaturated downdrafts. We do not call it FT air either, since it may originate from the cloudy layer.

1.3 Goal of the article

To acknowledge the diversity and complexity of mixing mechanisms, we extend the B15 framework in two ways. First, we assume that we know the relationship between δD and q in the FT, which allows us to get rid of one unknown. Second, we write the specific humidity of the air originating from above the SCL as a function of z_{orig}.

While B15 focused on observations during field campaign, we also apply the extended equation to global outputs an isotope-enabled general circulation model, with the aim to quantify the different factors controlling the δD variability at the global scale. The variable z_{orig} will emerge as an important factor. Therefore, we discuss the possibility that δD measurements at the near surface and through the lower FT could help estimate z_{orig}, and thus the mixing processes between the SCL and the air above.

Note that we focus on δD only. Results for $\delta^{18}O$ are similar. We do not aim at capturing second-order parameter d-excess, because our model requires some knowledge about free tropospheric vertical profiles of isotopic composition. While δD is known to decrease with altitude (Ehhalt, 1974; Ehhalt et al., 2005; Sodemann et al., 2017), vertical profiles of d-excess are more diverse and less well understood (Sodemann et al., 2017). In addition, the need for an extension of MJ79 is more needed for δD than for d-excess anyway, since MJ79 already performs quite well for d-excess (Risi et al., 2010d; Benetti et al., 2014).

Atmos. Chem. Phys. Discuss., https://doi.org/10.5194/acp-2019-254
Manuscript under review for journal Atmos. Chem. Phys.
Discussion started: 29 March 2019

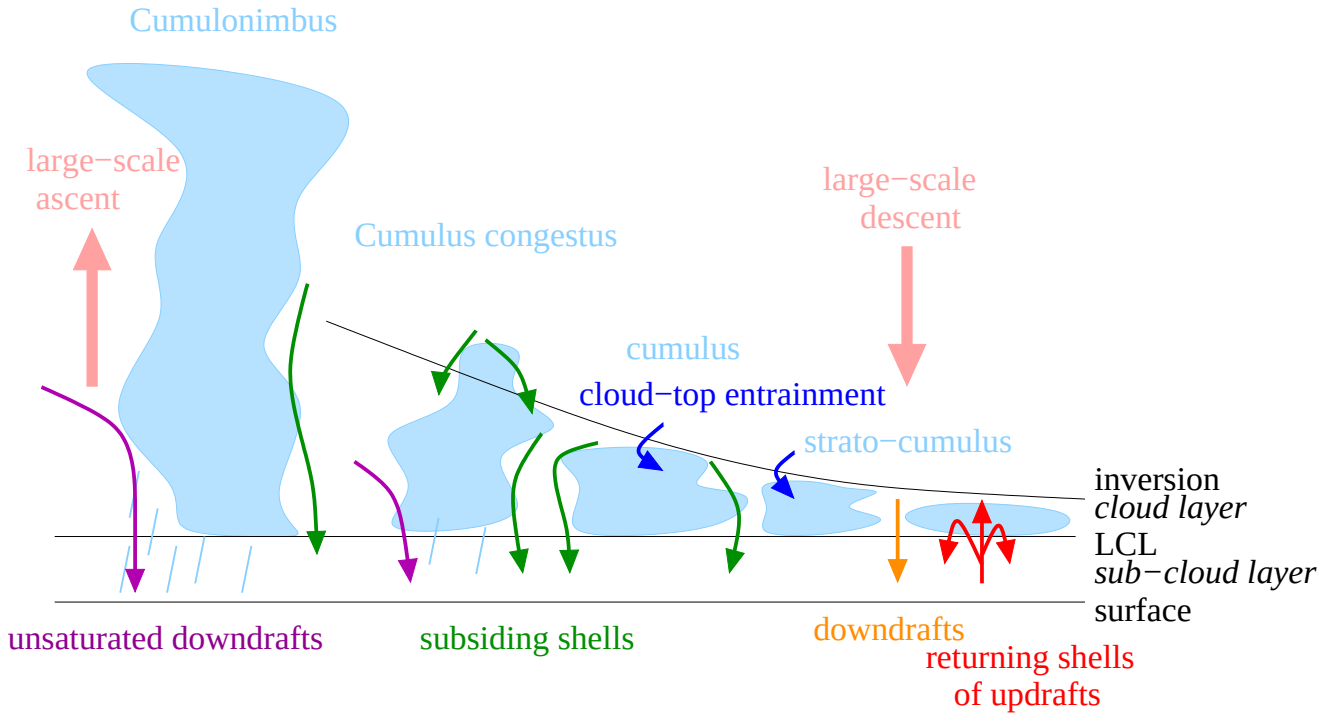

Figure 1. Schematics showing the different types of clouds and mixing processes as a function of the large-scale circulation.

2 Theoretical framework

2.1 Assumptions leading to the Benetti et al 2015 equation

In this section, we recall how the equation in Benetti et al. (2014) and B15 was derived and explicit all underlying assumptions.

We consider a simple box representing the SCL (Fig. 2). We assume that the air may come from above (M) or from the large-scale horizontal convergence ($D < 0$), and is exported through the SCL top (N, e.g. turbulent mixing or convective mass flux) or large-scale horizontal divergence ($D > 0$). We assume that the SCL is at steady state. In particular, its depth is constant. The air mass budget of the SCL thus writes:

$$M = N + D \tag{1}$$

These fluxes also transport water vapor and isotopes. In addition, surface evaporation E imports water vapor and isotopes (Fig. 2). We neglect import of water vapor and isotopes by rain evaporation (Albrecht, 1993) and will test the sensitivity to this effect in appendix B.

Hereafter, to simplify equations, we use the isotopic ratio R instead of δD.

Atmos. Chem. Phys. Discuss., https://doi.org/10.5194/acp-2019-254
Manuscript under review for journal Atmos. Chem. Phys.
Discussion started: 29 March 2019

Atmospheric Chemistry and Physics Discussions

The SCL is usually well-mixed (Betts and Ridgway, 1989; Stevens, 2006; De Roode et al., 2016), so that we can assume that the humidity and isotopic properties are constant vertically and horizontally in the SCL. They are noted (q_0, R_0). The humidity and isotopic properties of the mass flux export N are thus also (q_0, R_0). In case of net horizontal divergence ($D > 0$), the properties of the divergence flux are also (q_0, R_0). In case of net convergence ($D < 0$), we neglect large-scale horizontal gradients in air properties, so that the properties of the convergence flux are also (q_0, R_0). The properties of the flux M are noted (q_{orig}, R_{orig}) At steady state, the water budget of the SCL writes:

$$M \cdot q_{orig} + E = (N + D) \cdot q_0 \tag{2}$$

This model is consistent with SCL water budgets that have already been derived in previous studies (Bretherton et al., 1995), except that we consider steady state. This equation can be solved for q_0:

$$q_0 = q_{orig} + E/M \tag{3}$$

The SCL humidity q_0 is thus sensitive to M, justifying that it can be used to estimate the mixing intensity or the entrainment velocity $w_e = M/\rho_0$ (ρ being the air volumic mass) (Bretherton et al., 1995).

At steady state, the water isotope budget of the SCL writes:

$$M \cdot q_{orig} \cdot R_{orig} + E \cdot R_E = (N + D) \cdot q_0 \cdot R_0 \tag{4}$$

where R_E is the isotopic composition of the surface evaporation. It is assumed to follow the Craig and Gordon (1965) equation:

$$R_E = \frac{R_{oce}/\alpha_{eq} - h_0 \cdot R_0}{\alpha_K \cdot (1 - h_0)} \tag{5}$$

where R_{oce} is the isotopic ratio in the surface ocean water, α_{eq} is the equilibrium fractionation calculated at the ocean surface temperature (SST) (Majoube, 1971), α_K is the kinetic fractionation coefficient (MJ79) and h_0 is the relative humidity normalized at the SST ($h_0 = q_0/q_s(SST, P_0)$ where q_s is the specific humidity at saturation function and P_0 is the surface pressure).

By combining all these equations, we get:

$$R_0 = \frac{(1 - r_{orig}) \cdot R_{oce}/\alpha_{eq} + \alpha_K \cdot (1 - h_0) \cdot r \cdot R_{orig}}{(1 - r_{orig}) \cdot h_0 + \alpha_K \cdot (1 - h_0)} \tag{6}$$

where $r_{orig} = q_{orig}/q_0$ is the proportion of the water vapor in the SCL that originates from above.

Atmos. Chem. Phys. Discuss., https://doi.org/10.5194/acp-2019-254
Manuscript under review for journal Atmos. Chem. Phys.
Discussion started: 29 March 2019

Atmospheric Chemistry and Physics Discussions

An intriguing aspect of this equation is that the sensitivity to M disappears. In contrast to q_0, R_0 is not sensitive to M. Therefore, it appears illusory to promise that water vapor isotopic measurements could help constrain the entrainment velocity that many studies have strived to estimate (Nicholls and Turton, 1986; Khalsa, 1993; Wang and Albrecht, 1994; Bretherton et al., 1995; Faloona et al., 2005; Gerber et al., 2005, 2013). The lack of sensitivity of R_0 to M is explained physically by the fact that for a given q_0 and q_{orig}, if M increases, then E increases in the same proportion to maintain the water balance. Therefore, the proportion of the water vapor originating from surface evaporation and from above, to which R_0 is sensitive, remains constant. Rather, since q and R vary with altitude, R_0 is sensitive to the altitude from which the air originates, as argued in the next paragraph.

2.2 Two additional assumptions to close the equation

Equation (6) requires to know q_{orig} and R_{orig}. B15 closed it by taking the values of q_{orig} and R_{orig} at 700 hPa from GCM outputs. We modify this in two ways.

First, we want to acknowledge the diversity and complexity of mixing mechanisms by taking q_{orig} and R_{orig} at a variable altitude z_{orig}:

$$q_{orig} = h(z_{orig}) \cdot q_s(\bar{T}(z_{orig}) + \delta T(z_{orig}), P(z_{orig})) \tag{7}$$

where $\bar{T}(z_{orig}) + \delta T(z_{orig}) = T(z_{orig})$ is the temperature at altitude z_{orig}, $\bar{T}$ is the tropical-ocean-mean temperature profiles, $h(z_{orig})$ and $P(z_{orig})$ are the relative humidity and pressure at z_{orig}, and $\delta T(z_{orig})$ is the temperature perturbation compared to $\bar{T}$. Therefore, the unknown q_{orig} is replaced by the unknown z_{orig}.

Note that in all our equations, we assume that temperature and humidity profiles and all basic surface meteorological variables are known. We make no attempt to express h_0 as a function of q_0 as in B15. Our ultimate goal is to assess the added value of δD assuming that meteorological measurement are already routinely done. Therefore, variations of δD_0 that are mediated by q_0 or h_0 do not interest us.

Second, to deal with R_{orig} in Eq. (6) and get an analytical solution, we assume that the vertical profile of R follows a known relationship as a function of q. Measured vertical profiles of δD are usually bounded by two curves when plotted in a (q, δD) diagram (Sodemann et al., 2017): Rayleigh distillation curve and mixing line. We explore these two extreme cases in the next section and in appendix A respectively.

2.3 Closure if the tropospheric profile follows a Rayleigh line

Here we assume that R_{orig} is uniquely related to q_{orig} by Rayleigh distillation (Dansgaard, 1964), as in Galewsky and Rabanus (2016):

$$R_{orig} = R_0 \cdot r_{orig}^{\alpha_{eff}-1} \tag{8}$$

Atmos. Chem. Phys. Discuss., https://doi.org/10.5194/acp-2019-254
Manuscript under review for journal Atmos. Chem. Phys.
Discussion started: 29 March 2019

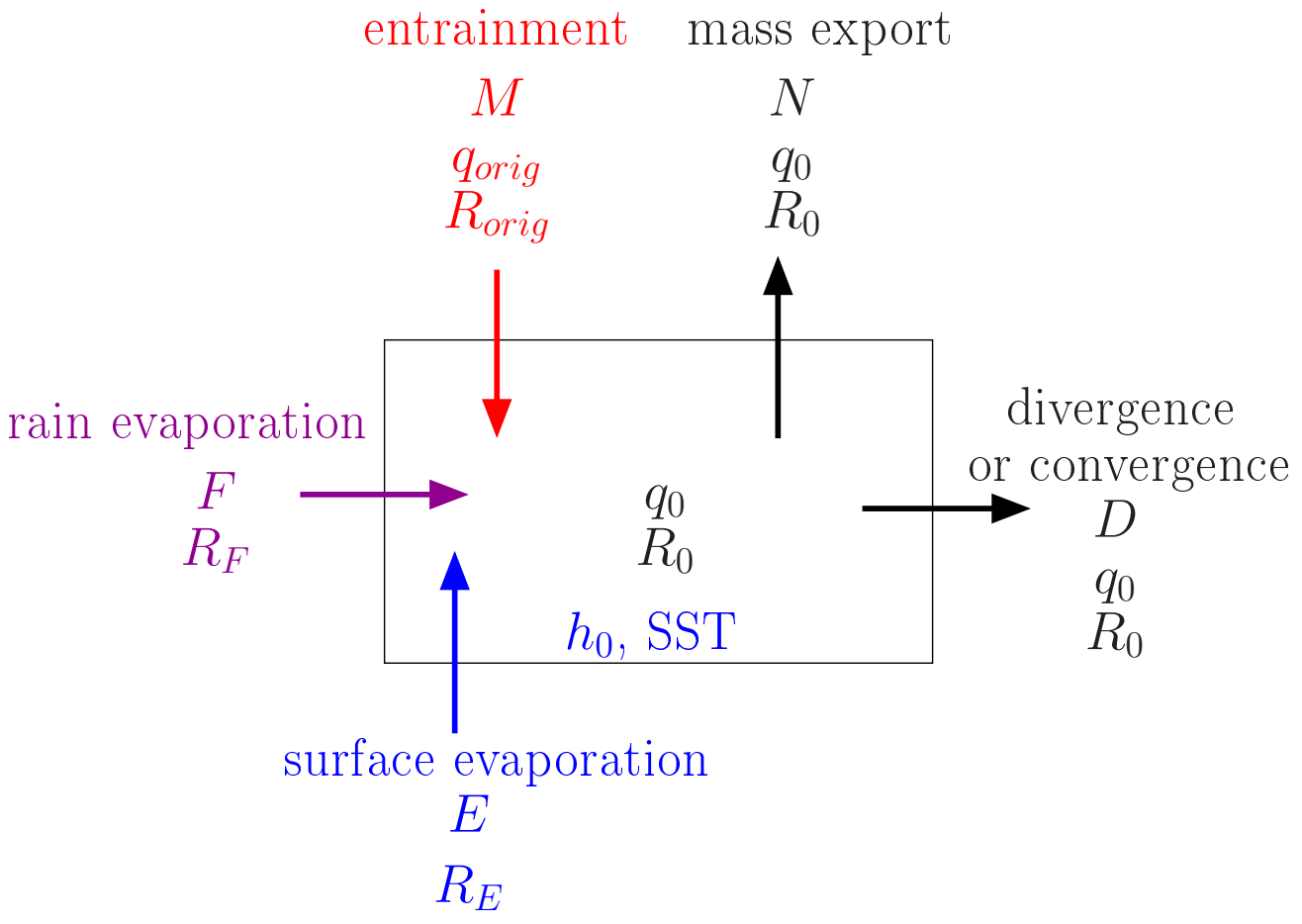

Figure 2. Schematics showing the simple box model on which the theoretical framework is based, and illustrating the main notations.

where α_{eff} is an effective fractionation coefficient. Typically, q decreases with altitude, so R also decreases with altitude. However, in observations and models, vertical profiles of R can be very diverse (Bony et al., 2008; Sodemann et al., 2017). The water vapor may be more (Worden et al., 2007) or less (Sodemann et al., 2017) depleted than predicted by Rayleigh curve using a realistic fractionation factor that depends on local temperature. Therefore, here we let α_{eff} be a free parameter larger than 1. Rather than assuming a true Rayleigh curve, we simply assume that R and q are logarithmically related.

Injecting Eq. (8) into Eq. (6), we get:

$$R_0 = \frac{R_{oce}}{\alpha_{eq}} \cdot \frac{1}{h_0 + \alpha_K \cdot (1-h_0) \cdot \frac{1-r_{orig}^{\alpha_{eff}}}{1-r_{orig}}} \tag{9}$$

Atmos. Chem. Phys. Discuss., https://doi.org/10.5194/acp-2019-254
Manuscript under review for journal Atmos. Chem. Phys.
Discussion started: 29 March 2019

Atmospheric Chemistry and Physics Discussions

As a consistency check, in the limit case where the air coming from above is totally dry ($r_{orig} = 0$), we find the MJ79 equation:

$$R_0 = \frac{R_{oce}}{\alpha_{eq}} \cdot \frac{1}{h_0 + \alpha_K \cdot (1 - h_0)} \tag{10}$$

Equation (9) tells us that whenever $\alpha_{eff} > 1$, R_0 decreases as r_{orig} increases (Fig. 3 red), i.e. as q_{orig} is moister. Therefore, R_0 decreases as z_{orig} is lower in altitude. This result may be counter-intuitive, but can be physically interpreted as follows. If z_{orig} is high, mixing brings air with very depleted water vapor, but since the air is dry, the depleting effect is small. In contrast, if z_{orig} is low, mixing brings air with water vapor that is not very depleted, but since the air is moist, the depleting effect is large (Fig. 4a).

Figure 3 (red) shows that the range of possible δD values is restricted to -70 ‰ to -85 ‰. This explains why in quiescent conditions near the sea level in tropical ocean locations, the water vapor δD varies little Benetti et al. (2014) (F. Vimeux pers. comm.). In the limit case where $r_{orig} \to 1$ (i.e. the air comes from the SCL top), $R_0 \to \frac{R_{oce}}{\alpha_{eq}} \cdot \frac{1}{h_0 + \alpha_K \cdot (1-h_0) \cdot \alpha_{eff}}$. This lower bound is not so depleted compared to the more depleted water vapor observed in regions of deep convection (e.g. Lawrence et al. (2002); Lawrence et al. (2004); Kurita (2013)). This is because when $r_{orig} \to 1$, the water vapor coming from above has a composition very close to that of the SCL, so the depleting effect is limited. In addition, surface evaporation strongly damps the depleting effect of mixing. Only rain evaporation or liquid-vapor exchanges (Lawrence et al., 2004; Worden et al., 2007) can further decrease R_0 (appendix B).

Figure 3 (green) shows that the sensitivity to α_{eff} is relatively small but cannot be neglected. Therefore, predicting water vapor δD requires to have some knowledge about the steepness of the isotopic profiles in the FT.

Assuming a Rayleigh shape for the δD profile allows us to find a good-looking analytical solution, but our main results (more depleted δD_0 as r_{orig} increases, restricted range of δD_0 variations, relationship with z_{orig}) would hold for any δD profile that is steeper than the mixing line. If the profile follows as mixing line, however, our results would not hold any more, because no single end member can be identified, as illustrated in Fig. 4b and analytically demonstrated in appendix A. Therefore, in the remaining of the paper, we will assume that R follows a logarithmic line. We will assess the validity of this assumption in section 4.1.

An important assumption that led to Eq. (9) is the neglect of SCL moistening by rain evaporation. We propose an extended equation including rain evaporation in appendix B). Rain evaporation can have a depleting or enriching effect (e.g. pink and blue curves in Fig. 3), depending on microphysical details that are too complex to be addressed here. Therefore, we neglect rain evaporation effects and our results will be valid only in regions covered by non-precipitating clouds, e.g. subsiding regions covered by non-precipitating trade-wind cumulus, strato-cumulus or stratus clouds.

Atmos. Chem. Phys. Discuss., https://doi.org/10.5194/acp-2019-254
Manuscript under review for journal Atmos. Chem. Phys.
Discussion started: 29 March 2019

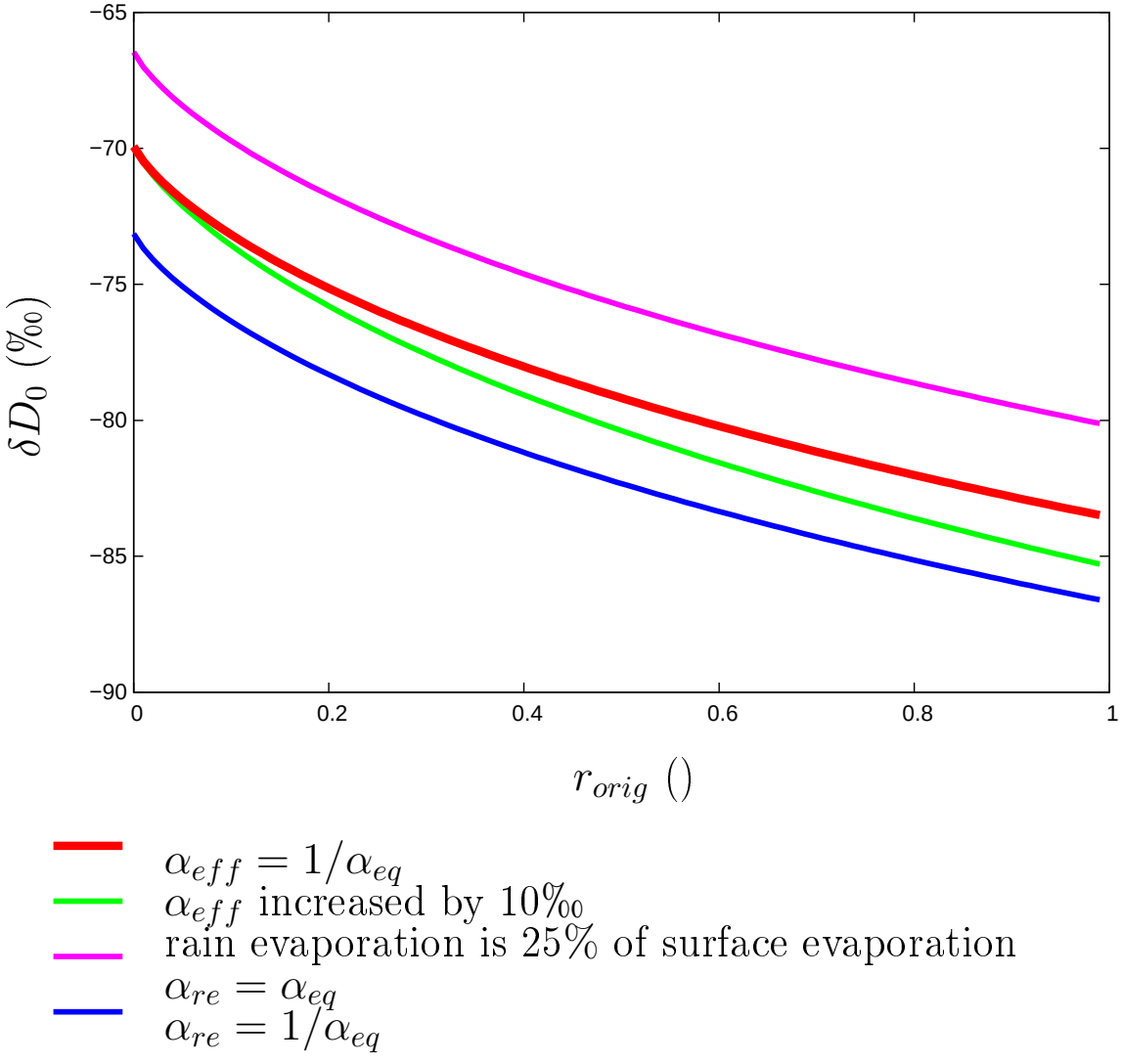

Figure 3. δD_0 as a function of r_{orig} according to Eq. (9), with $\alpha_{eff} = \alpha_{eq}$ as an example (red). The sensitivity to the effective fractionation factor α_{eff} (green) is shown. In case of rain evaporation fractionation, the sensitivity to the effective fractionation factor α_{re} (see appendix B) is shown (pink, blue).

Atmos. Chem. Phys. Discuss., https://doi.org/10.5194/acp-2019-254
Manuscript under review for journal Atmos. Chem. Phys.
Discussion started: 29 March 2019

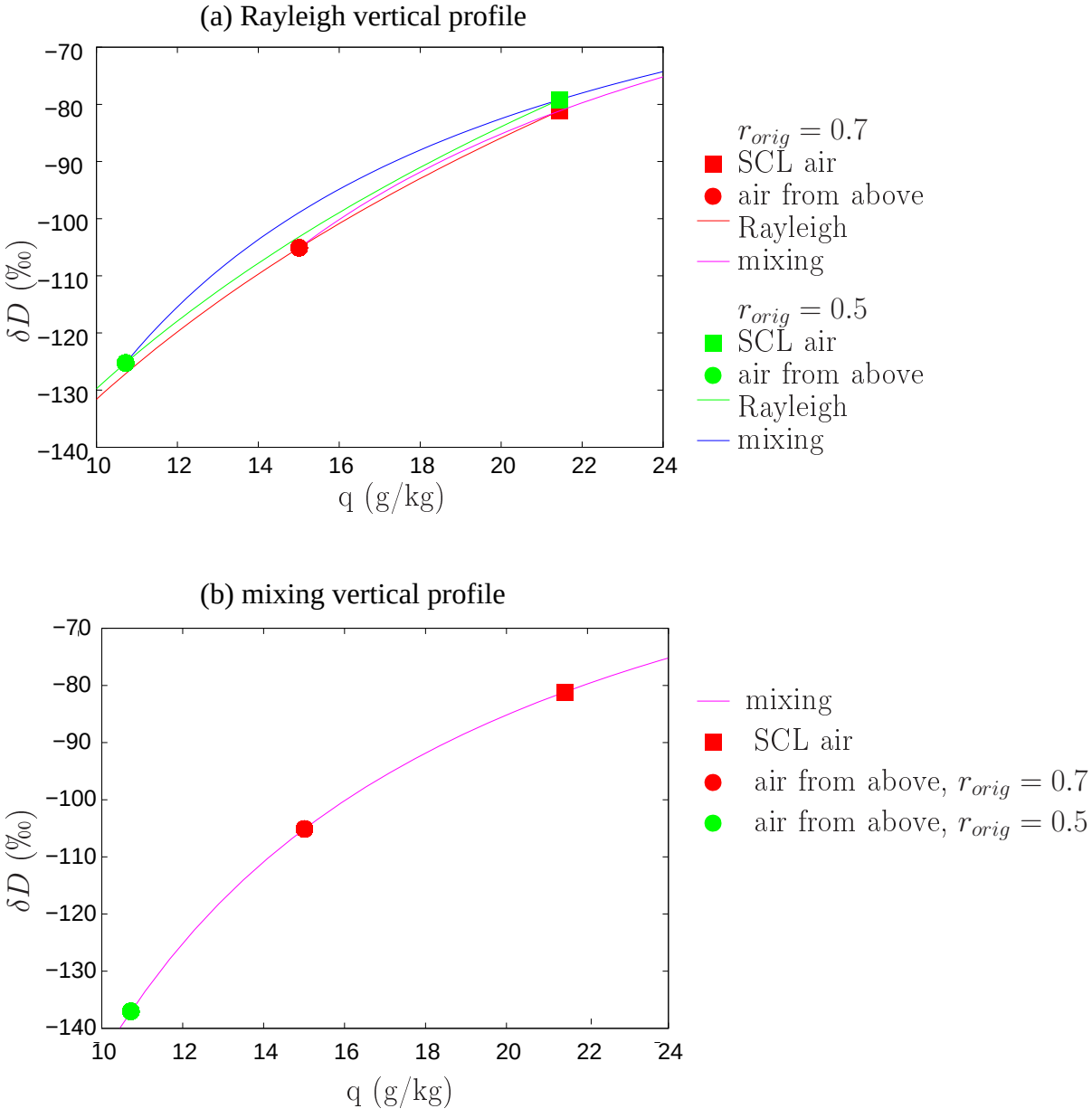

Figure 4. Idealized $q - \delta D$ diagrams showing how the SCL water vapor δD is set. (a) If δD profiles follow Rayleigh distillation. The red curve shows the Rayleigh profile starting from the SCL and the pink curve shows the mixing line connecting the air coming from above to the surface evaporation, in the case $r_{orig} = q_{orig}/q_0 = 0.7$. The green curve shows the the Rayleigh profile starting from the SCL and the blue curve shows the mixing line connecting the air coming from above to the surface evaporation, in the case $r_{orig} = q_{orig}/q_0 = 0.5$. One can visually see that when r_{orig} is lower, the mixing line is more curved, leading to more enriched values. (b) If δD profiles follow a mixing line. The pink curve joins the SCL air and the air at all altitudes above the SCL. One can see that different values for r_{orig} can lead to the same value of δD in the SCL.

Atmos. Chem. Phys. Discuss., https://doi.org/10.5194/acp-2019-254
Manuscript under review for journal Atmos. Chem. Phys.
Discussion started: 29 March 2019

Atmospheric Chemistry and Physics Discussions

3 Model simulations, observations and methods

3.1 LMDZ simulations

We use an isotope-enabled general circulation model (GCM) as a laboratory to test our hypotheses and investigate isotopic controls. We use the LMDZ5A version of LMDZ (Laboratoire de Météorologie Dynamique Zoom), which is the atmospheric component of the IPSL-CM5A coupled model (Dufresne et al., 2012) that took part in CMIP5 (Coupled Model Intercomparison Project, Taylor et al. (2012)). This version is very close to LMDZ4 (Hourdin et al., 2006). Water isotopes are implemented the same way as in its predecessor LMDZ4 (Risi et al., 2010c). We use 4 years (2009-2012) of an AMIP (Atmospheric Model Intercomparison Project)-type simulation (Gates, 1992) that was initialized in 1977. The winds are nudged towards ERA-40 reanalyses (Uppala et al., 2005) to ensure a more realistic simulation. Such a simulation has already been described and extensively validated for isotopic variables in both precipitation and water vapor (Risi et al., 2010c, 2012a). The ocean surface water δD_{oce} is assumed constant and set to 4 ‰. The resolution is 2.5° in latitude × 3.75° in longitude, with 39 vertical levels. Over the ocean, the first layer extends up to 64 m, and a typical SCL extending up to 600 m is resolved by 6 layers. Around 2500 m, a typical altitude for the inversion for trade-wind cumulus clouds, the resolution is about 500 m.

3.2 STRASSE observations

We also apply our theoretical framework to observations during the STRASSE (subtropical Atlantic surface salinity experiment) cruise that took place in the Northern subtropical ocean in August and September 2012 (Benetti et al., 2014). This campaign accumulates several advantages that are important for our analysis: (1) continuous δD_0 measurements in the surface water vapor (17m) at a high temporal frequency during one month (Benetti et al., 2014, 2015, 2017b), (2) associated surface meteorological measurements, including SST and h_0, (3) 22 radio-soundings relatively well distributed over the campaign period and providing vertical profiles of altitude, temperature, relative humidity and pressure, (4) ocean surface water δD_{oce} measurements (Benetti et al., 2017a), (5) a variety of conditions ranging from quiescent weather to convective conditions, (6) on many vertical profiles, a well defined temperature inversion allows to calculate the inversion altitude.

We use δD_0 measurements on a 15-minute time step. The measurements in ocean water were interpolated on the same time steps using a Gaussian filter with a width of 3 days. The radio-soundings are used together with all water vapor isotopic measurements that are within 30 minutes of the radio-sounding launch. Only profiles during the ascending phase of the balloon are considered.

3.3 Estimating the altitude from which the air originates

First, α_{eff} is estimated assuming that (q_f, δD_f) at 500hPa follows a Rayleigh distillation from the surface:

$$\alpha_{eff} = 1 + \frac{ln(R_f/R_0)}{ln(q_f/q_0)}$$

Atmos. Chem. Phys. Discuss., https://doi.org/10.5194/acp-2019-254
Manuscript under review for journal Atmos. Chem. Phys.
Discussion started: 29 March 2019

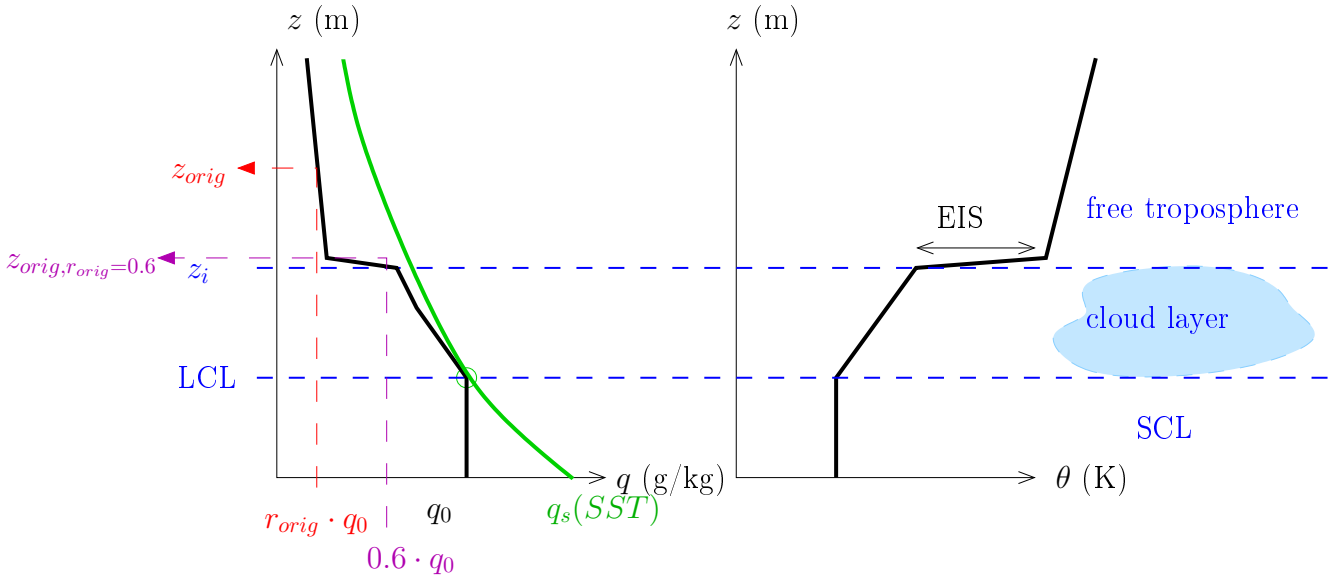

Figure 5. Schematics illustrating the typical structure of tropical marine boundary layers. Left: shape of the vertical profile in q (black) and q_s (green). Right: shape of the vertical profile in potential temperature θ, inspired by Wood and Bretherton (2006). The LCL, z_{orig} , $z_{orig,r_{orig}=0.6}$ and z_i altitudes defined in section 3.4 are indicated.

We checked that results are similar when defining the end member at 400 hPa rather than 500 hPa. However, if the end member is defined below 500 hPa (e.g. 600 hPa), results are not always reasonable.

Second, r_{orig} is estimated based on Eq. (9), using α_{eff}, α_{eq}, α_K , δD_{oce}, h_0 and δD_0.

Third, the altitude z_{orig} is estimated from r_{orig}. Using the q vertical profile, we find z_{orig} so that $q(z_{orig}) = r_{orig} \cdot q_0$ (Fig. 5, red).

Note that if assumptions underlying Eq. (9) are violated, then the estimate of r_{orig}, and subsequently z_{orig}, will be based. The estimate of r_{orig} encapsulates the effect of mixing processes, but also all other processes that have been neglected in our theoretical framework, such as temporal variations in SCL depth, q_0 or δD_0, horizontal gradients in q_0 or δD_0, or rain evaporation. For example, in case of deep convection, depleting rain evaporation will reflect into an artificially larger r_{orig} and lower z_{orig}. We have to keep this in mind when interpreting the results.

3.4 Boundary layer structure diagnostics

Figure 5 illustrates the structure of a typical tropical marine boundary layer covered by strato-cumulus or cumulus clouds (Betts and Ridgway, 1989; Wood, 2012; Wood and Bretherton, 2004; Neggers et al., 2006; Stevens, 2006). The cloud base corresponds to the lifting condensation level (LCL). Below is the well-mixed SCL. Above is the cloud layer, topped by a temperature inversion. Above the inversion is the FT.

Atmos. Chem. Phys. Discuss., https://doi.org/10.5194/acp-2019-254
Manuscript under review for journal Atmos. Chem. Phys.
Discussion started: 29 March 2019

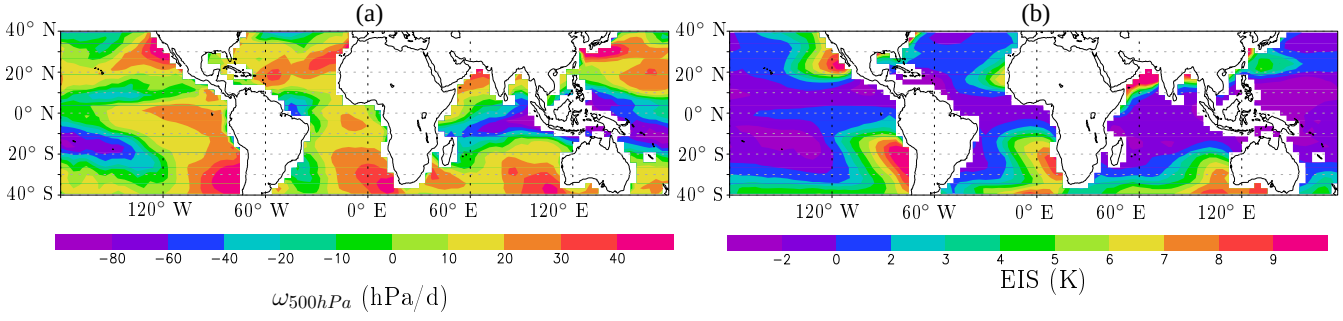

Figure 6. Maps of winter-mean ω_{500} (a) and EIS (b) simulated by LMDZ.

The LCL is calculated as the altitude at which the specific humidity near the surface equals the specific humidity at saturation of a parcel that is lifted following a dry adiabat (Fig. 5). In LMDZ, the inversion altitude z_i is calculated as the first level at which the vertical potential temperature gradients exceeds 3 times the moist-adiabatic lapse rate. In observations, z_i is calculated as the first level at which the vertical potential temperature gradients exceeds 5 times the moist-adiabatic lapse rate, because radio-soundings are noisier than simulated profiles. These estimates are consistent with what we would estimate from visual inspection of vertical profiles. Finally, we calculate $z_{orig,r_{orig}=0.6}$, which is the z_{orig} altitude if r_{orig} is set to 0.6. This usually coincides with the altitude of strong humidity decrease near the inversion (Fig. 5).

3.5 Averages and composites

All calculations are done on daily values for LMDZ, and on 15-minute values for observations.

For LMDZ, when analyzing spatial and seasonal variability, seasonal averages are calculated at each grid box by averaging all days of all years that belong to each season. Seasons are defined as boreal winter (December-January-February), spring (March-April-May), summer (June-July-August) and fall (September-October-November). For illustration purpose, all maps are plotted for boreal winter. Standard deviations are also calculated among all days of all years for each season.

The type of clouds and mixing processes depends strongly on the large-scale velocity at 500 hPa (ω_{500}, Fig. 6a), with shallow clouds in subsiding regions and deeper clouds in ascending regions ((Bony et al., 2004), Fig. 1). Therefore, composites are calculated by averaging all seasonal-mean values at all locations that belong to a given interval of ω_{500}.

The cloud cover strongly depends on the inversion strength, with increasing cloud fraction as inversion strength increases. We use Estimated Inversion Strength (EIS) (Wood and Bretherton, 2006) (Fig. 6b) as a measure of inversion strength. Composites as a function of EIS are calculated by averaging all seasonal-mean values at all locations that belong to a given interval of EIS.

3.6 Decomposition method for δD_0

To understand what controls the δD_0 spatio-temporal variations, δD_0 is decomposed into 4 contributions based on Eq. (9). The 4 factors, r_{orig}, α_{eff}, SST and h_0, are alternatively varied each one at a time, assuming that all other factors are constant

Atmos. Chem. Phys. Discuss., https://doi.org/10.5194/acp-2019-254
Manuscript under review for journal Atmos. Chem. Phys.
Discussion started: 29 March 2019

Atmospheric Chemistry and Physics Discussions

($r_{orig} = 0.6$, $\alpha_{eff} = 1.09$, SST=25°C, $h_0 = 0.8$). This yields 4 components, representing the effects of the variability of r_{orig}, α_{eff}, SST and h_0 on δD_0.

The relative contribution of each of these effects to the δD variability is quantified by performing a linear regression of each of the components as a function of δD_0. If the correlation coefficient is significant for a given factor, then the slope quantifies the contribution of this factor to the variability of δD_0. The sum of all contributions may not always be 1 due to non-linearity. Such a method has already been applied in previous studies (e.g.Risi et al. (2010b); Oueslati et al. (2016)). The contributions to the seasonal-spatial variability of δD_0 can be quantified by performing the regression among all locations and seasons. The contributions to the daily variability of δD_0 can be quantified by performing the regression among all days of a given season at a given location.

3.7 Decomposition method for r_{orig}

To understand what controls r_{orig}, a similar method can be applied, based on Eq. (7):

$$r_{orig} = \frac{h(z_{orig}) \cdot q_s(\bar{T}(z_{orig}) + \delta T(z_{orig}), P(z_{orig}))}{q_0} \tag{11}$$

Therefore, the variability of r_{orig} is decomposed into the effect of 4 factors: q_0, z_{orig}, $h(z_{orig})$ and $\delta T(z_{orig})$. In practice, r_{orig} and z_{orig} are calculated following section 3.3, then Eq. (11) is applied.

4 Results from LMDZ

4.1 Does the tropospheric profile follow a mixing or Rayleigh line?

First, we test whether the δD vertical profiles simulated by LMDZ follow a Rayleigh or mixing curve as a function of q. For the Rayleigh curve, α_{eff} is estimated as explained in section 3.3. For the mixing line, the end member (q_f, R_f) is also taken at 500 hPa. Examples of vertical δD profiles simulated by LMDZ and predicted by the Rayleigh and mixing lines are plotted in Fig. 7. We can see that simulated profiles are usually bounded by these two extreme lines, consistent with observations (Sodemann et al., 2017). Profiles are however much smoother than in observations, due to the coarse vertical resolution of the model. The coarse vertical resolution is a limitation to keep in mind when discussing the shape of vertical profiles.

When assuming a Rayleigh or mixing curve, the root mean square error (RMSE) on the δD profile from the surface to 500hPa ranges from 5 to 30 ‰ (Fig. 8a-b). In average, RMSE are slightly larger for Rayleigh, but this depends on the location and no generic curve fits perfectly well the vertical profiles. This is consistent with the diversity of observed profile shapes (Sodemann et al., 2017). In the following, we will assume that the Rayleigh curve is a good first order approximation. Our method of z_{orig} estimate remains valid even if δD vertical profiles do not follow Rayleigh, as long they follow a curve that is steeper than mixing. This is the case in LMDZ (Fig. 7).

Atmos. Chem. Phys. Discuss., https://doi.org/10.5194/acp-2019-254
Manuscript under review for journal Atmos. Chem. Phys.
Discussion started: 29 March 2019

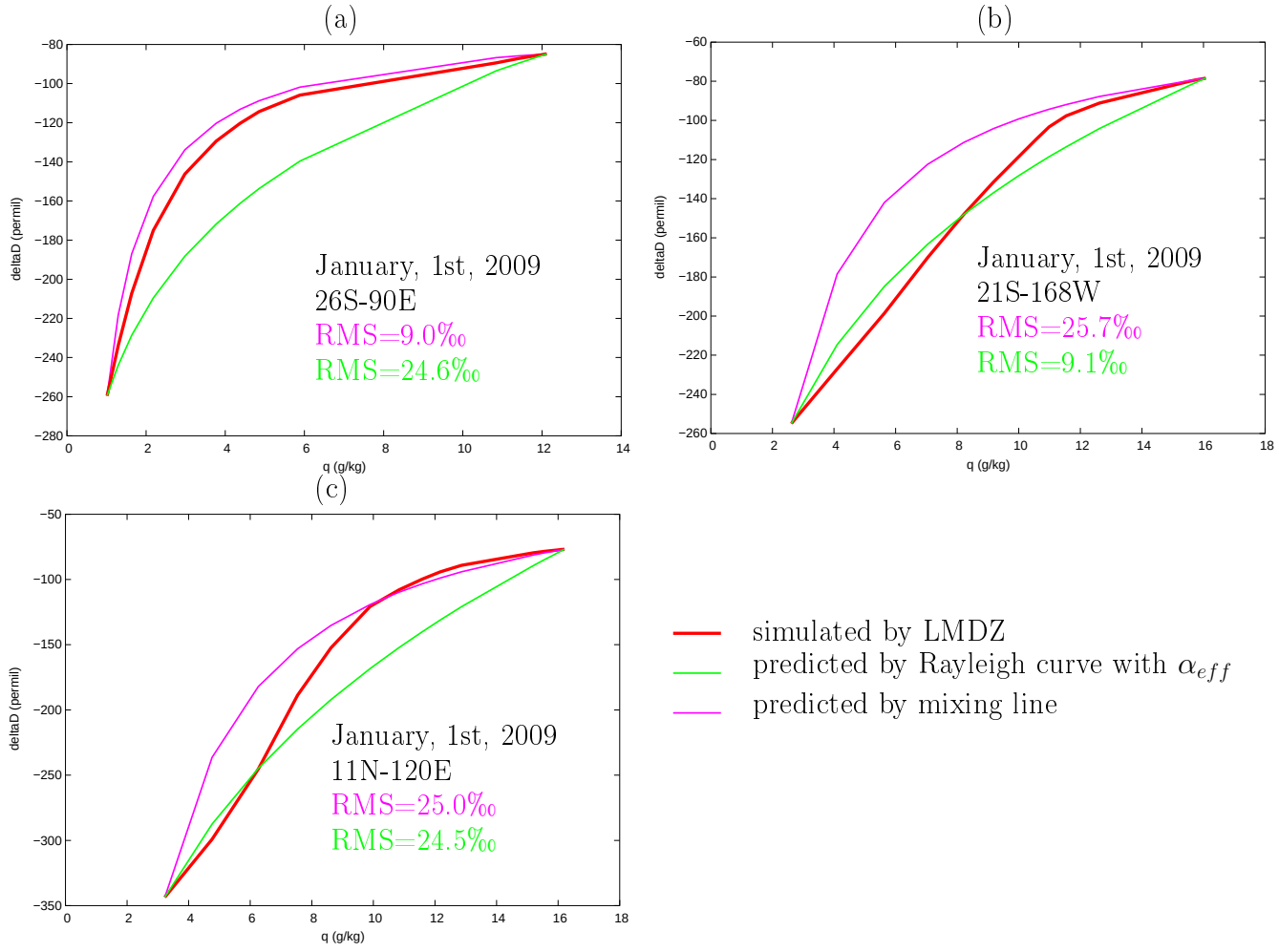

Figure 7. Examples of vertical profiles simulated by LMDZ (red), predicted by a Rayleigh curve with α_{eff} estimated to fit the simulated δD at 500 hPa (section 3.3, green), and predicted by a mixing line with the dry end member at 500 hPa (pink). Three examples are given: (a) the simulated profile is closed to a mixing line, (b) the simulated profile is closed to a Rayleigh line, and (c) the simulated profile deviates both from a mixing and a Rayleigh line (c). The RMS values indicate the RMS difference between simulated profile and mixing line (pink) or Rayleigh curve (green).

Figure 8c shows the estimated α_{eff} . It is maximum in regions of deep convection. This is consistent with the maximum depletion simulated in deep convective regions in the mid-troposphere simulated by models (Bony et al., 2008), leading to steeper δD profiles. The pattern of α_{eff} may also reflect horizontal advection effects (Dee et al., 2018).

Values α_{eff} are of the same order of magnitude as real fractionation factors, but the spatial variations do not reflect those predicted if using a fractionation coefficient α_{eq} a function of temperature T (Fig. 8f). Rayleigh curves using $\alpha_{eq}(T)$ poorly predict vertical profiles of δD (Fig. 8c), with RMSE values exceeding 20 ‰ at most locations.

Atmos. Chem. Phys. Discuss., https://doi.org/10.5194/acp-2019-254
Manuscript under review for journal Atmos. Chem. Phys.
Discussion started: 29 March 2019

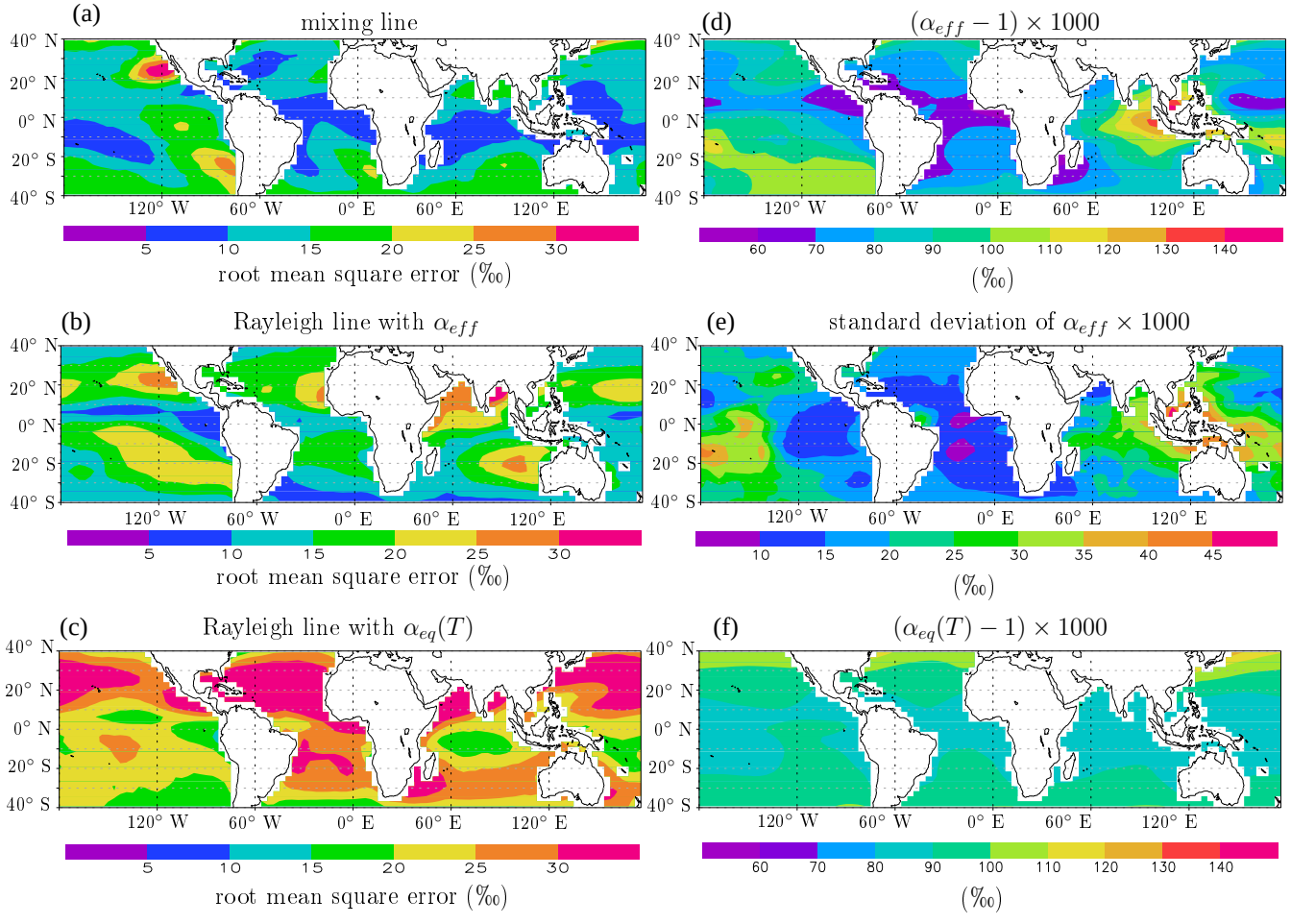

Figure 8. a) Root mean square error (RMSE) between the simulated δD profile and a δD profile that would follow a mixing curve between the surface and 500 hPa. b) Same as a but for a profile that would follow a Rayleigh curve between the surface and 500 hPa, with α_{eff} determined based on simulated δD at 500 hPa. c) Same as b but for a profile that would follow a Rayleigh curve using equilibrium fractionation calculated as a function of temperature, $\alpha_{eq}(T)$. d) $\alpha_{eff} - 1$, where α_{eff} is the effective fractionation coefficient, expressed in ‰. e) Standard deviation of α_{eff} among all days in winter of all years, expressed in ‰. f) $\alpha_{eq}(T) - 1$ expressed in ‰. For a-d and f, all daily values are averaged over all days in winters of all years.

Atmos. Chem. Phys. Discuss., https://doi.org/10.5194/acp-2019-254
Manuscript under review for journal Atmos. Chem. Phys.
Discussion started: 29 March 2019

Atmospheric Chemistry and Physics Discussions

4.2 Decomposition of δD_0 variability

The spatial variations of δD_0 simulated by LMDZ (Fig. 9a) are characterized by depleted values near mid-latitudes and in dry subsiding regions (e.g. off the coast of Peru and over other upwelling regions) and in deep convective regions (e.g. Maritime Continent). Consistently, δD_0 values exhibit a maximum for weakly ascending or subsiding regions: δD_0 decreases as ω_{500} is more strongly ascending or descending (Fig. 10a black); δD_0 decreases as EIS increases reflecting more stable, subsiding conditions (Fig. 10b black). This pattern is consistent with previous studies (e.g. Good et al. (2015)). For the first time, we propose a theoretical framework to interpret this pattern, decomposing it into 4 contributions: r_{orig}, α_{eff}, SST and h_0 (section 3.6). We check that the reconstructed δD_0 from the sum of its 4 contributions is very similar to the simulated δD_0 (Fig. 9b, 10 dashed black).

In ascending regions, the main contribution explaining the more depleted δD_0 in deep convective regions is that of α_{eff} (Fig. 9d, 10a red). α_{eff} is higher in more ascending regions. This means that the main factor depleting δD_0 in deep convective regions is the fact that the mid-troposphere is more depleted. This leads to a steeper gradient (higher α_{eff}), and thus a more efficient depletion by vertical mixing. This is consistent with deep convection depleting the water vapor most efficiently in the mid-troposphere (Bony et al. (2008)). The second main contribution is that associated with r_{orig}(Fig. 9c, 10a green). r_{orig} is larger in deep convective regions. However, we recall that Eq. (9) does not consider rain evaporation, which is a significant source of water vapor in deep convective regions (Worden et al. (2007)). Rain evaporation in deep convective regions is expected to deplete the water vapor (section B), so that neglecting rain evaporation leads to an over-estimate of r_{orig} in these regions. Therefore, the stronger r_{orig} in deep convective regions could be partially an artifact reflecting the effect of rain evaporation.

In subsidence regions, the main factor explaining the more depleted δD_0 as subsidence is stronger, or as EIS increases, is the cold SST (Fig. 9e, 10a pink), leading to larger α_{eq}, and to a lesser extent the dry h_0 (Fig. 9f, 10a purple). The contribution of r_{orig} is also a significant contribution to the depletion of δD_0 in the cold upwelling regions (Fig. 9c). In subsidence regions, r_{orig}, is unlikely to be an artifact of rain evaporation there, and probably really reflect the importance of mixing processes. The shallower boundary layer there are associated with higher r_{orig}. The fact that the effect of r_{orig} can be seen on the composites as a function of EIS (Fig. 10b, green) and not as a function of ω_{500} may reflect the fact that EIS reflects more faithfully the cloud and mixing processes in dry, stable regions than ω_{500} does (Wood and Bretherton, 2006).

From a quantitative point of view, we can decompose the δD_0 seasonal-spatial variations into these different effects (section 3.6). In regions of large-scale ascent, α_{eff} is the main factor explaining the δD_0 seasonal-spatial variations (37 %), followed by r_{orig} (17 %) (Table 1). In regions of large-scale descent, SST is the main factor explaining the seasonal-spatial variations (54 %), followed by r_{orig} (16 %) and α_{eff} (14 %) (table 1).

The decomposition method can also be applied to decompose the δD_0 variability at the daily time scale at each location and for each season. On average, in ascending regions, r_{orig} is the main factor (49 %), followed by α_{eff} (39 %). In subsiding regions, the effect of SST is muted due to its slow variability, and r_{orig} (59 %), α_{eff} (49 %) and h_0 (62 %) become the main factors.

Atmos. Chem. Phys. Discuss., https://doi.org/10.5194/acp-2019-254
Manuscript under review for journal Atmos. Chem. Phys.
Discussion started: 29 March 2019

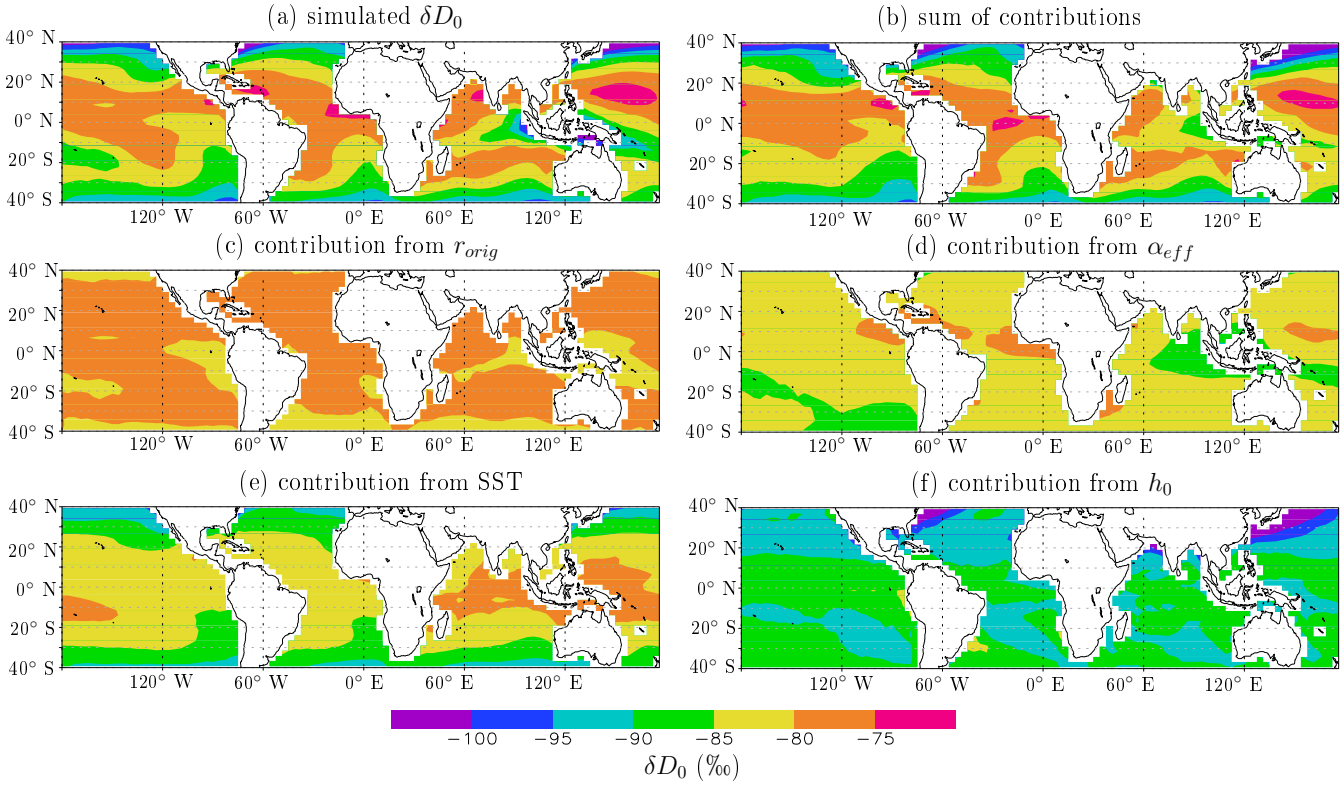

Figure 9. a) Map of winter-mean δD_0 simulated by LMDZ. b) Map of winter-mean δD_0 reconstructed as the sum of the 4 contributions. Note that to focus on variations only and to get values of the same order of magnitude as the simulated δD_0 field, we subtracted the mean of the 4 contributions and added the mean of simulated δD_0 to the reconstructed δD_0 field. c) Map of winter-mean δD_0 calculated from Eq. (9) if only r_{orig} varies (see section 3.6). d) Same as b but of only α_{eff} varies. e) Same as b but if only SST varies. f) Same as b but if only h_0 varies.

Overall, results highlight the importance of r_{orig} as one of the main factors controlling the spatio-temporal variability of δD_0.

4.3 Decomposition of r_{orig} variability

Given the importance of r_{orig} in controlling the δD_0 variations, we now decompose r_{orig} into its 4 contributions: q_0, z_{orig}, h_{orig} and δT_{orig} (section 3.6). Spatially, r_{orig} is maximum in regions of strong large-scale ascent (Fig. 12a) such as the Maritime continent (Fig. 11a), and in very stable regions (Fig. 12b) such as upwelling regions (Fig. 12a). We check that the reconstructed r_{orig} from the sum of its 4 contributions is very similar to the simulated r_{orig} (Fig. 11b, 12 dashed black).

In regions of strong large-scale ascent, r_{orig} is larger mainly because h_{orig} is larger (Fig. 11e, 12a pink). This suggests that even though the effect of rain evaporation may artificially bias high the estimate of r_{orig} , a substantial part of the r_{orig}

Atmos. Chem. Phys. Discuss., https://doi.org/10.5194/acp-2019-254
Manuscript under review for journal Atmos. Chem. Phys.
Discussion started: 29 March 2019

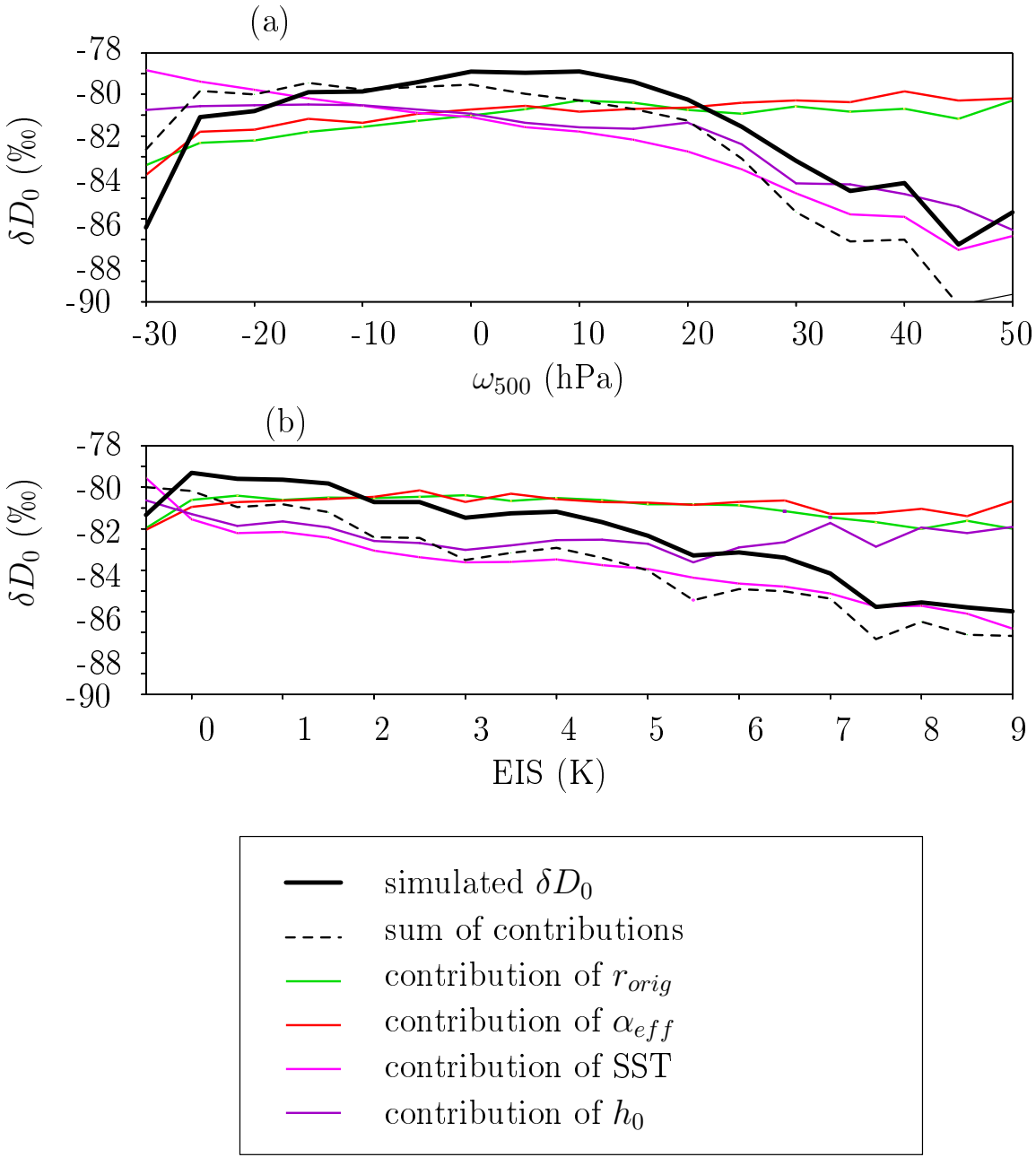

Figure 10. Composites as a function of ω_{500} (a) and of EIS (b) of the seasonal averages of δD_0 simulated by LMDZ over all tropical ocean locations (black). Same for the sum of the contributions (black dashed) and for each individual contribution to δD_0: r_{orig} varies (green), α_{eff} (red), SST (pink) and h_0 (purple).

Atmos. Chem. Phys. Discuss., https://doi.org/10.5194/acp-2019-254
Manuscript under review for journal Atmos. Chem. Phys.
Discussion started: 29 March 2019

Atmospheric Chemistry and Physics Discussions

Regime	ascending		Subsiding	
	correlation coefficient	slope	correlation coefficient	slope
r_{orig}	0.71	0.17	0.50	0.16
α_{eff}	0.75	0.37	0.36	0.14
SST	-0.20	-0.06	0.89	0.54
h_0	0.09	0.03	0.35	0.23

Table 1. Decomposition of the spatial and seasonal variation in δD_0 into its 4 contributions: effect of r_{orig}, α_{eff}, SST and h_0 variations. For each contribution, we show the correlation coefficient of the linear regression of the contribution as a function of δD_0. The threshold for the correlation coefficient to be statistically significant at 99 % is 0.15 or lower in all cases. The analysis is done separately for ascending and subsiding regimes. All seasons and tropical oceans locations are considered.

Regime	Ascending		Subsiding	
	correlation coefficient	slope	correlation coefficient	slope
q_0	-0.24	0.0	0.09	0.0
z_{orig}	0.88	0.61	0.65	0.72
h_{orig}	0.75	0.94	0.53	0.91
δT_{orig}	0.33	0.12	-0.34	-0.27

Table 2. Decomposition of the spatial-seasonal variation in r_{orig} into its 4 contributions: effect of q_0, z_{orig}, h_{orig} and δT_{orig} variations. For each contribution, we show the correlation coefficient of the linear regression of the contribution as a function of r_{orig}. The threshold for the correlation coefficient to be statistically significant is 0.15 or lower in all cases. The analysis is done separately for ascending and subsiding regimes. All seasons and tropical oceans locations are considered.

signal is actually physical. Indeed, if the large r_{orig} was purely an artifact of the neglect of rain evaporation, it would translate totally into a lower z_{orig}. Physically, the moister the FT, the higher the contribution of vapor coming from above to the vapor of the SCL, and thus the higher r_{orig} and the more depleted δD_0. This mechanism through which a moister FT leads to a more depleted δD_0 is consistent with that argued in B15.

In very stable regions, r_{orig} is larger mainly because q_0 is small (Fig. 11c, 12b green), consistent with the drier conditions in these regions of large-scale descent, and because z_{orig} is lower in altitude (Fig. 11d, 12b red), consistent with the shallower boundary layers as EIS increases. Physically, the lower in altitude the air comes from, the higher r_{orig} and the more depleted δD_0. This mechanism was not considered in Benetti et al. (2015) but our decomposition shows that it is a key mechanism driving r_{orig} and thus δD_0 variations in stable regions.

Quantitatively, in ascending regions, the main factors controlling the seasonal-spatial variations in r_{orig} are h_{orig} (94 %) and z_{orig} (61 %) (Table 2). Similarly, in descending regions, the main factors are also h_{orig} (91 %) and z_{orig} (72 %) (Table 2). At the daily scale, the same two factors dominate the variability of r_{orig}: h_{orig} and z_{orig} contribute to 67 % and 76 % of r_{orig} variations in average over ascending regions, and to 104 % and 73 % in average over descending regions.

Atmos. Chem. Phys. Discuss., https://doi.org/10.5194/acp-2019-254
Manuscript under review for journal Atmos. Chem. Phys.
Discussion started: 29 March 2019

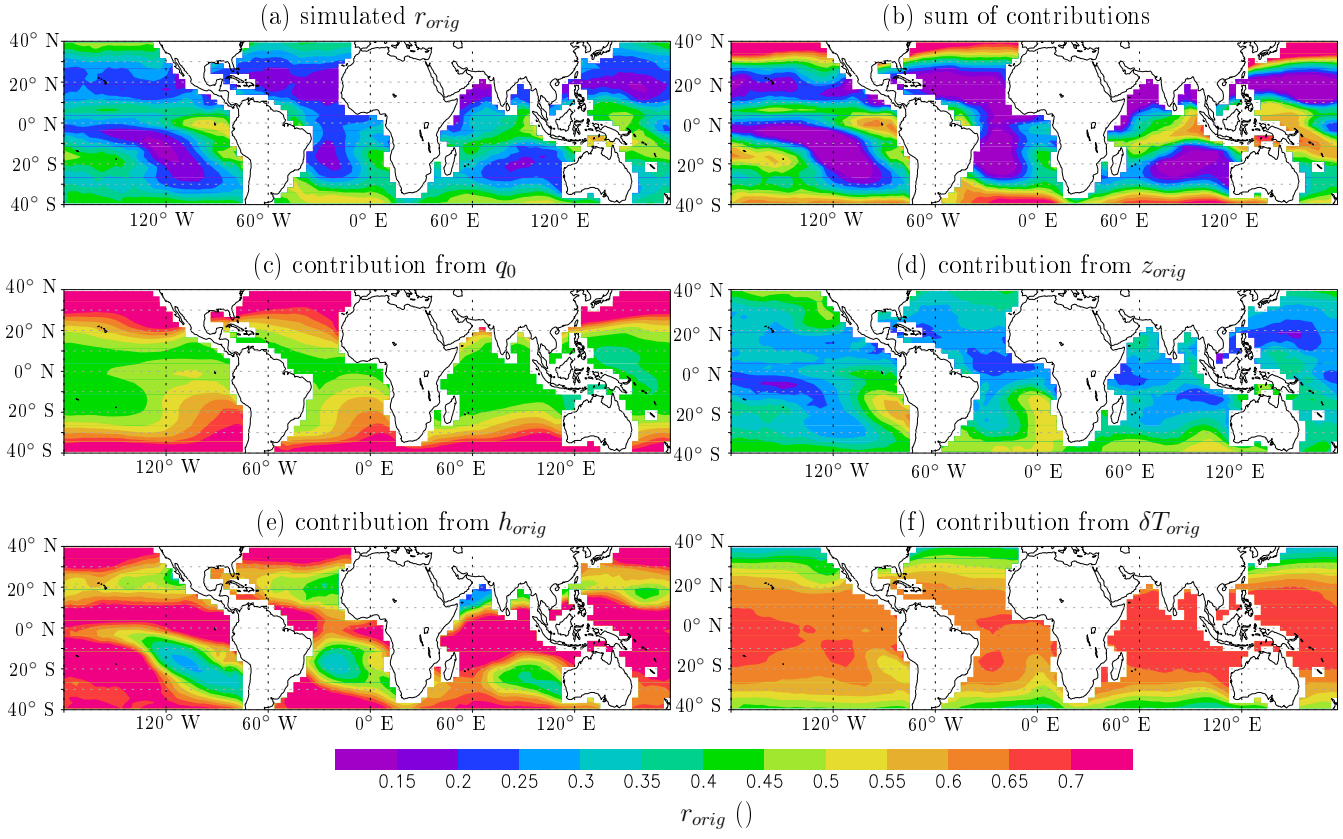

Figure 11. a) Map of winter-mean r_{orig} simulated by LMDZ. b) Map of winter-mean r_{orig} reconstructed as the sum of the 4 contributions. c) Map of winter-mean r_{orig} calculated from Eq. (11) if only q_0 varies (see section 3.6). d) Same as b but of only z_{orig} varies. e) Same as b but if only $h(z_{orig})$ varies. f) Same as b but if only δT_{orig} varies.

4.4 Entrainment altitude estimate

Estimated altitude z_{orig} is minimum in dry subsiding regions, especially in upwelling regions (Fig. 13a, Fig. 14), corresponding to regions with strongest inversion (Fig. 13). This contributes to the depleted δD_0 in these regions.

As explained in 3.3, our estimate of z_{orig} may be artificially biased due to the neglect of some processes in our theoretical framework. Ideally, to check whether z_{orig} really physically represents the altitude from which the air originates, additional model experiments where water vapor from different levels are tagged (Risi et al., 2010b) would be needed. While we leave this for future work, in the meanwhile we check whether z_{orig} estimates are consistent with what we expect based on what we know about mixing processes in the marine boundary layers. We expect that in strato-cumulus regions, air is entrained from a very shallow (a few tens of meters) layer above the inversion, whereas the mixing processes may be more diverse, and possibly deeper in the FT, as the boundary layer deepens (Fig. 1).

Atmos. Chem. Phys. Discuss., https://doi.org/10.5194/acp-2019-254
Manuscript under review for journal Atmos. Chem. Phys.
Discussion started: 29 March 2019

Atmospheric Chemistry and Physics Discussions

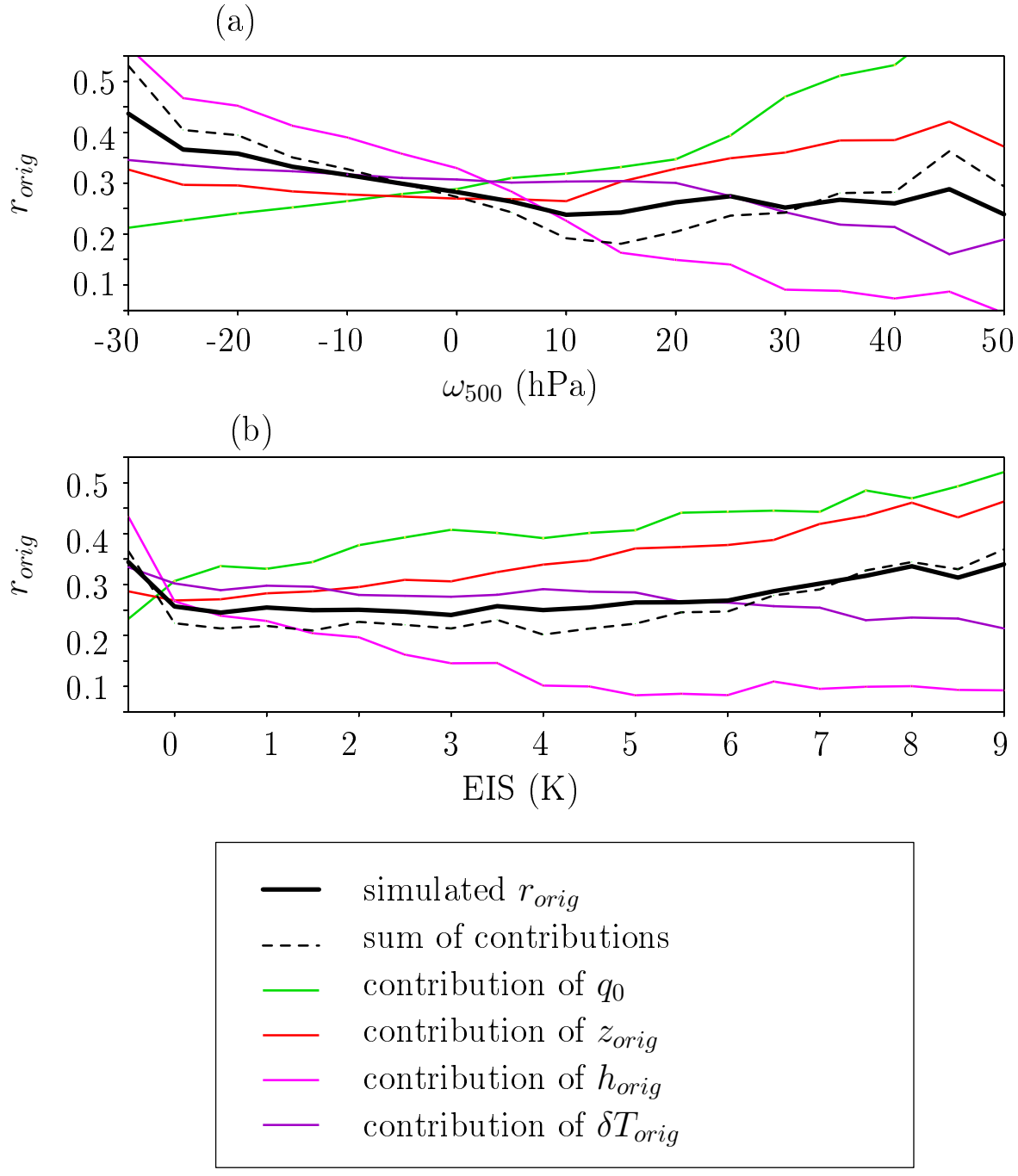

Figure 12. Composites as a function of ω_{500} (a) and of EIS (b) of the seasonal averages of r_{orig} simulated by LMDZ over all tropical ocean locations (black). Same for the sum of the contributions (black dashed) and for each individual contribution to r_{orig} : q_0 varies (green), z_{orig} (red), $h(z_{orig})$ (pink) and δT_{orig} (purple).

Atmos. Chem. Phys. Discuss., https://doi.org/10.5194/acp-2019-254
Manuscript under review for journal Atmos. Chem. Phys.
Discussion started: 29 March 2019

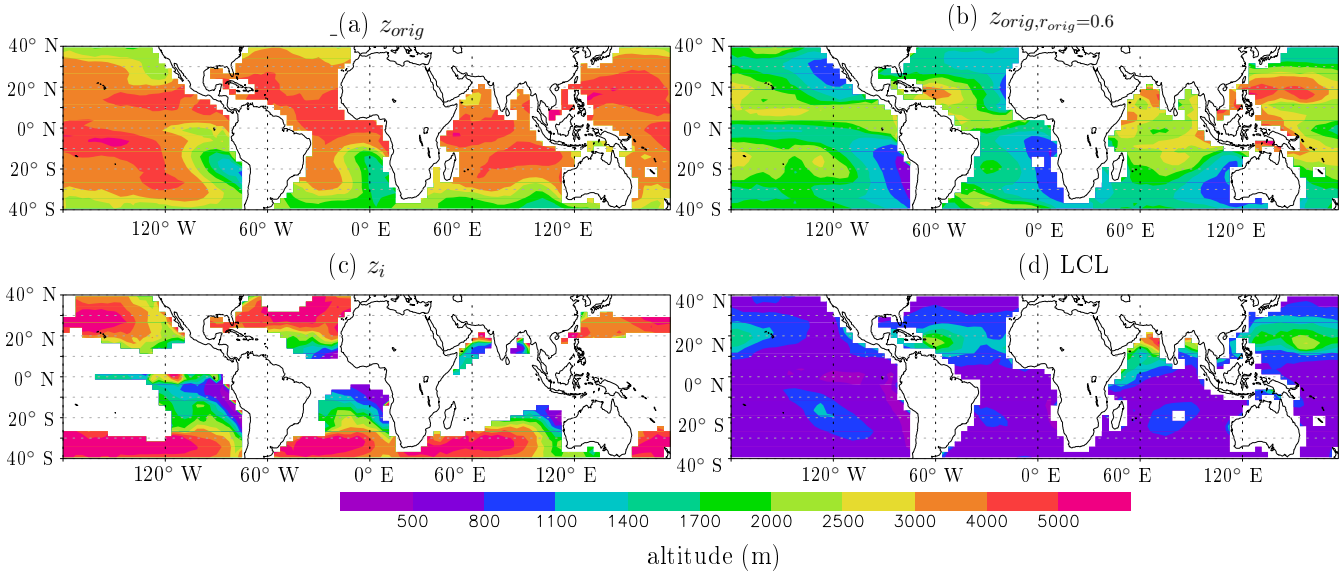

Figure 13. a) Map of winter-mean z_{orig} estimated from δD_0 simulated by LMDZ. b) Same as a but z_{orig} that we would estimate if r_{orig} was constant set to 0.6 ($z_{orig,r_{orig}=0.6}$). c). Same as a but for z_i simulated from LMDZ. Only days when EIS>2 K are considered, otherwise z_i is difficult to estimate. d) Same as a but for LCL simulated by LMDZ.

To check whether estimated z_{orig} is consistent with this picture, we compare z_{orig} to $z_{orig,r_{orig}=0.6}$ (z_{orig} that we would estimate is r_{orig} was set constant to 0.6) and z_i (section 3.4), which are measures of the altitude of the humidity drop and temperature inversion respectively. As expected from Fig. 1, they are minimum in dry upwelling regions, intermediate in trade-wind regions, and maximum values in convective regions (Fig. 13c-d, 14 green, blue). Therefore, the low z_{orig} in upwelling regions reflects the low z_i. Consistently, in subsiding regions, z_{orig} correlates well with $z_{orig,r_{orig}=0.6}$ (correlation coefficient of 0.52, statistically significant beyond 99 %). If we focus on very stable regions only (EIS>7 K), z_{orig} correlates well with both $z_{orig,r_{orig}=0.6}$ and z_i (correlation coefficient of 0.58 and 0.52 respectively, statistically significant beyond 99 %). The altitude z_{orig} is a few meters above the inversion in strato-cumulus regions, and up to 1km above the inversion in cumulus and deep convective regions (Fig. 14), consistent with our expectations from Fig. 1. This lends support to the fact that at least in subsiding regions, our isotope-based z_{orig} estimate effectively reflect the origin of air coming from above.

In ascending regions, in contrast, z_{orig} does not correlate significantly with $z_{orig,r_{orig}=0.6}$ or z_i. This may indicate either that our z_{orig} estimate is biased by neglected processes such as rain evaporation, or that in deep convective regions, the origin of FT air into the SCL is very diverse due to the variety of mixing processes (1).

Atmos. Chem. Phys. Discuss., https://doi.org/10.5194/acp-2019-254
Manuscript under review for journal Atmos. Chem. Phys.
Discussion started: 29 March 2019

Atmospheric Chemistry and Physics Discussions

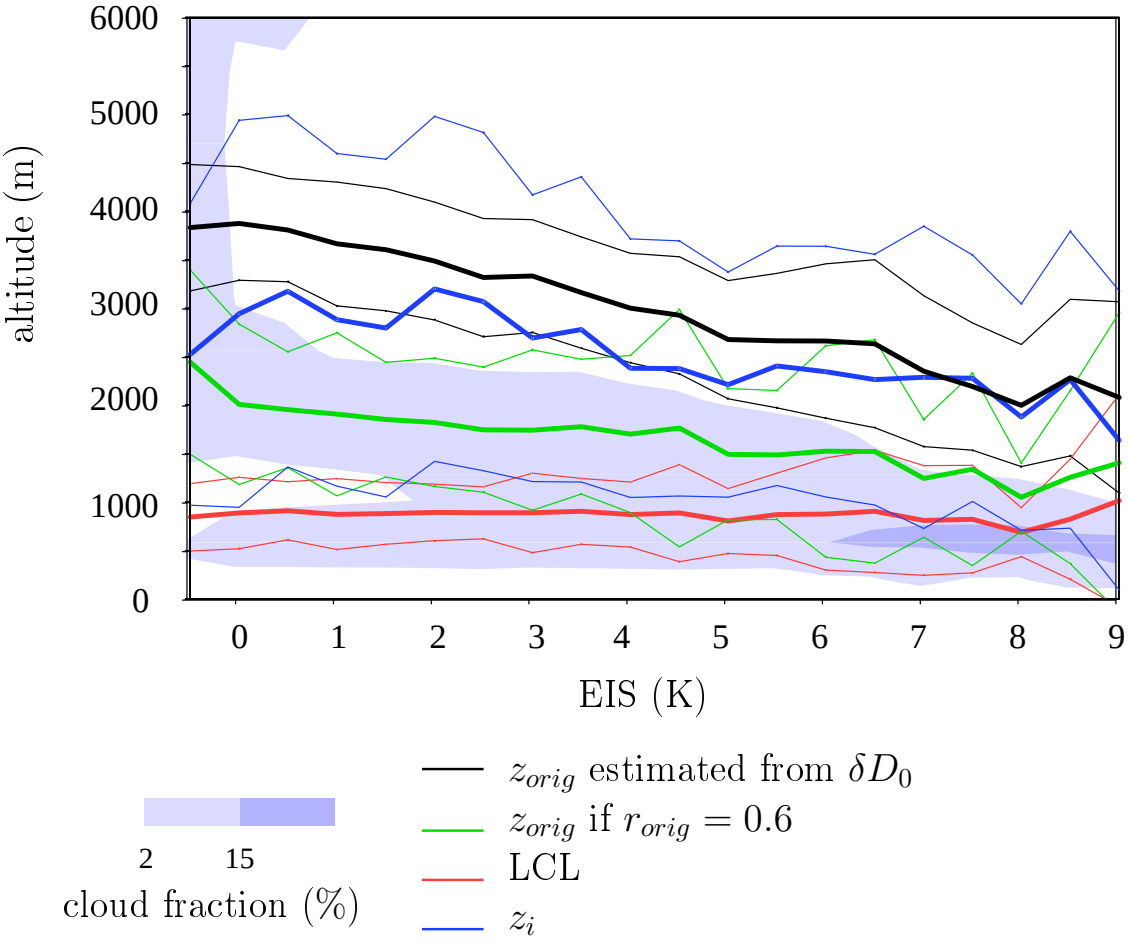

Figure 14. Composites as a function of EIS of seasonal-mean of z_{orig} (black), $z_{orig,r_{orig}=0.6}$ (green), z_i (blue) and LCL (red). The composite profiles of cloud cover are also shown, showing deep clouds when EIS is close to 0 and shallowest clouds when EIS is largest.

5 Results from observations

To check whether our results obtained with LMDZ are realistic, we apply our methods to the measurements gathered during the STRASSE campaign. In the absence of measured δD profiles, we assume that α_{eff} is 1.07 based on LMDZ simulation.

Throughout the cruise, δD_0 shows a large variability, ranging from around -75 ‰ in quiescent conditions to -120 ‰ during the two convective conditions (Benetti et al., 2014) (Fig. 15a red). Variability in r_{orig} is the major factor contributing to this variability (58 %) (Fig. 15a green, Table 3). This crucial importance of mixing processes is consistent with B15.

During the two convective events, the estimated r_{orig} saturates at 1 (Fig. 15b). This proves that r_{orig} estimated in these conditions is biased high because it encapsulates the effect of neglected processes, i.e. depletion by rain evaporation. Equation (9) is not valid in this case. In addition, at the scale of a few hours, the steady-state assumptions may be violated. Rain

Atmos. Chem. Phys. Discuss., https://doi.org/10.5194/acp-2019-254
Manuscript under review for journal Atmos. Chem. Phys.
Discussion started: 29 March 2019

Atmospheric Chemistry and Physics Discussions

contributions to δD_0	correlation coefficient	slope
r_{orig}	0.77	0.58
SST	0.57	0.16
h_0	0.40	0.48

Table 3. Same as Table 1 but for the STRASSE observations. Linear regressions are calculated among 1977 data points.

contributions to r_{orig}	correlation coefficient	slope
q_0	-0.46	-1.49
z_{orig}	0.66	0.90
h_{orig}	0.81	0.70
δT_{orig}	-0.36	-0.91

Table 4. Same as Table 2 but for the STRASSE observations. Linear regressions are calculated among 55 data points, so that correlation coefficients above 0.35 are statistically significant at 99 %.

evaporation may strongly deplete the SCL before surface evaporation has the time to play its dampening role, hence the possibility to reach very low δD_0 that cannot be predicted even when considering rain evaporation (appendix B).

During the rest of the cruise, the main factors controlling the r_{orig} variability are z_{orig} (90 %) and h_{orig} (70 %). The importance of FT humidity in controlling r_{orig} was already highlighted in B15. However, in their paper, the variability in z_{orig} was neglected, whereas it appears here as the main factor.

Through September, the cruises goes from a shallow boundary layer in early September to deeper boundary layers with higher inversions, before reaching the convective conditions (Fig. 15c). Consistently with this deepening boundary layer, the air is entrained from increasingly higher in altitude. When considering only the 6 data points when z_{orig} <2000 m, z_{orig} coincides almost exactly with z_i (Fig. 15c; the correlation coefficient between z_{orig} and z_i is 0.996). This indicates that the air is entrained into the SCL exactly from the inversion layer. Even if the number of sample is small, the coincidence is remarkable, especially when recalling that z_{orig} and z_i are estimated from completely independent observations. This lends support to the fact that our z_{orig} estimate is physical.

6 Discussion: what can we learn from water isotopes on mixing processes?

We have shown in the previous section that one of the main factors controlling δD_0 at the seasonal-spatial and daily scale are the proportion of the water vapor in the SCL that is originates from above (r_{orig}), and that one of the main factor controlling r_{orig} is the altitude from which the air originates (z_{orig}). In turn, could we use water vapor isotopic measurements to constrain z_{orig}? This would open the door to discriminating between different mixing processes at play (Fig. 1). Since mixing processes are crucial to determine the sensitivity of cloud fraction to SST (Sherwood et al., 2014; Bretherton, 2015; Vial et al., 2016), such a prospect would allow us to improve our knowledge of cloud feedbacks, and hence of climate sensitivity.

Atmos. Chem. Phys. Discuss., https://doi.org/10.5194/acp-2019-254
Manuscript under review for journal Atmos. Chem. Phys.
Discussion started: 29 March 2019

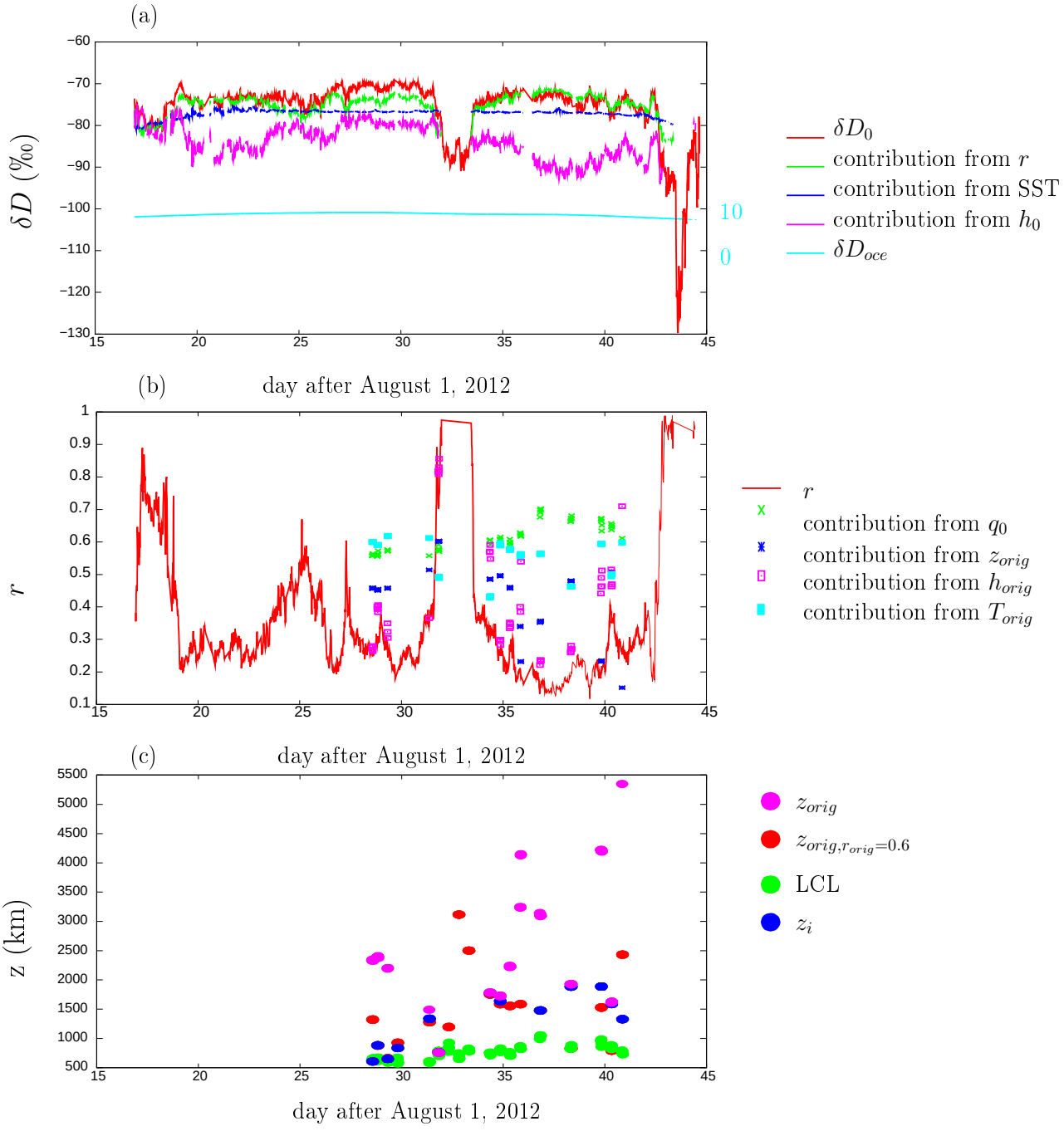

Figure 15. a) Time series of δD_0 observed during the STRASSE cruise, together with its 4 contributions. The δD of the surface ocean water is also plotted with the scale on the right. b) Time series of r_{orig} estimated from observations during the STRASSE campaign, together with its 4 contributions. c) Times series of z_{orig}, $z_{orig,r_{orig}=0.6}$, LCL and z_i estimated from the STRASSE observations.

Atmos. Chem. Phys. Discuss., https://doi.org/10.5194/acp-2019-254
Manuscript under review for journal Atmos. Chem. Phys.
Discussion started: 29 March 2019

Atmospheric Chemistry and Physics Discussions

With this in mind, we assess the errors associated with z_{orig} estimates from δD_0 measurements, and discuss whether there are small enough for z_{orig} estimates to be useful. In strato-cumulus clouds where the air is believed to be entrained from the first few tens of meters above cloud top (Faloona et al., 2005; Mellado, 2017), z_{orig} estimates are not useful if the errors are larger than a few tens of meters, e.g. 20 m. In cumulus clouds where mixing processes are more diverse and possibly deeper (Fig. 1), z_{orig} estimates may be useful if errors are of the order of 80 m.

Let's assume that we have a field campaign where we measure δD_0, surface meteorological variables, temperature and humidity profiles (e.g. radio-soundings), and a few δD profiles (e.g. by aircraft). This is what we can expect for example from the future EUREC4A (Elucidating the role of clouds-circulation coupling in climate) campaign to study trade-wind cumulus clouds (Bony et al., 2017).

The first source of uncertainty that we have highlighted in this article is the effect of rain evaporation. As long as the microphysical processes and associated isotopic fractionation processes are not well constrained, it is safer to restrain z_{orig} estimates to non-precipitating clouds.

The second source of uncertainty is the variability in α_{eff}. Measuring daily δD profiles is costly and difficult (Sodemann et al., 2017). Let's assume that we have only one profile that represents the seasonal-average at a given location. The daily standard deviation of α_{eff} ($\sigma_{\alpha_{eff}}$) for a given season ranges from 5‰ in the Central Atlantic to 40‰ near the Maritime Continent (Fig. 8d). To estimate the resulting error on z_{orig}, we re-estimate z_{orig} every day and at each location using $\bar{\alpha_{eff}} + \sigma_{\alpha_{eff}}$ and $\bar{\alpha_{eff}} - \sigma_{\alpha_{eff}}$. The error on z_{orig} is calculated as $\left(z_{orig}(\bar{\alpha_{eff}} - \sigma_{\alpha_{eff}}) - z_{orig}(\bar{\alpha_{eff}} + \sigma_{\alpha_{eff}})\right)/2$. The averaged error and its standard deviation is plotted as a function of EIS in Fig. 16 (black). It is of the order of 400m, and rarely below 200m. If we attempt to estimate α_{eff} as the fractionation coefficient as a function of local temperature, errors would be even more dissuasive (Fig. 16 blue).

Therefore, estimating z_{orig} from δD_0 measurements cannot be useful unless we measure daily δD profiles. Practically, we could imagine measuring FT properties (δD_f) at the top of a mountain while we measure δD_0 at the sea level (e.g. on Islands such as Hawaii or La Réunion, Galewsky et al. (2007); Bailey et al. (2013); Guilpart et al. (2017)). We could also imagine retrieving α_{eff} from daily δD profiles retrieved from space by IASI (Infrared Atmospheric Sounding Interferometer, Lacour et al. (2012, 2015)), but this would be associated with additional errors whose estimate is beyond the scope of this paper.

The third source of uncertainty are measurements errors. We recalculate z_{orig} assuming an error of 0.4 ‰ on δD_0 (typical of what we can measure with in-situ laser instruments, Benetti et al. (2014)) and 1 ‰ on δD_f (larger errors due to lower humidity and the increased complexity of measurements in altitude). Whereas errors on δD_f lead to errors on z_{orig} of the order of 20 m (Fig. 16, green), errors on δD_0 lead to errors on z_{orig} of the order of 80 m. This is higher than the upper bound for the expected entrainment altitude in strato-cumulus. Therefore, δD_0 measurements would need to be more accurate than usual to be useful in strato-cumulus regions, i.e. 0.1 ‰ to yield a 20 m precision on z_{orig}. In trade-wind cumulus regions, the precision is enough for z_{orig} to be useful.

Atmos. Chem. Phys. Discuss., https://doi.org/10.5194/acp-2019-254
Manuscript under review for journal Atmos. Chem. Phys.
Discussion started: 29 March 2019

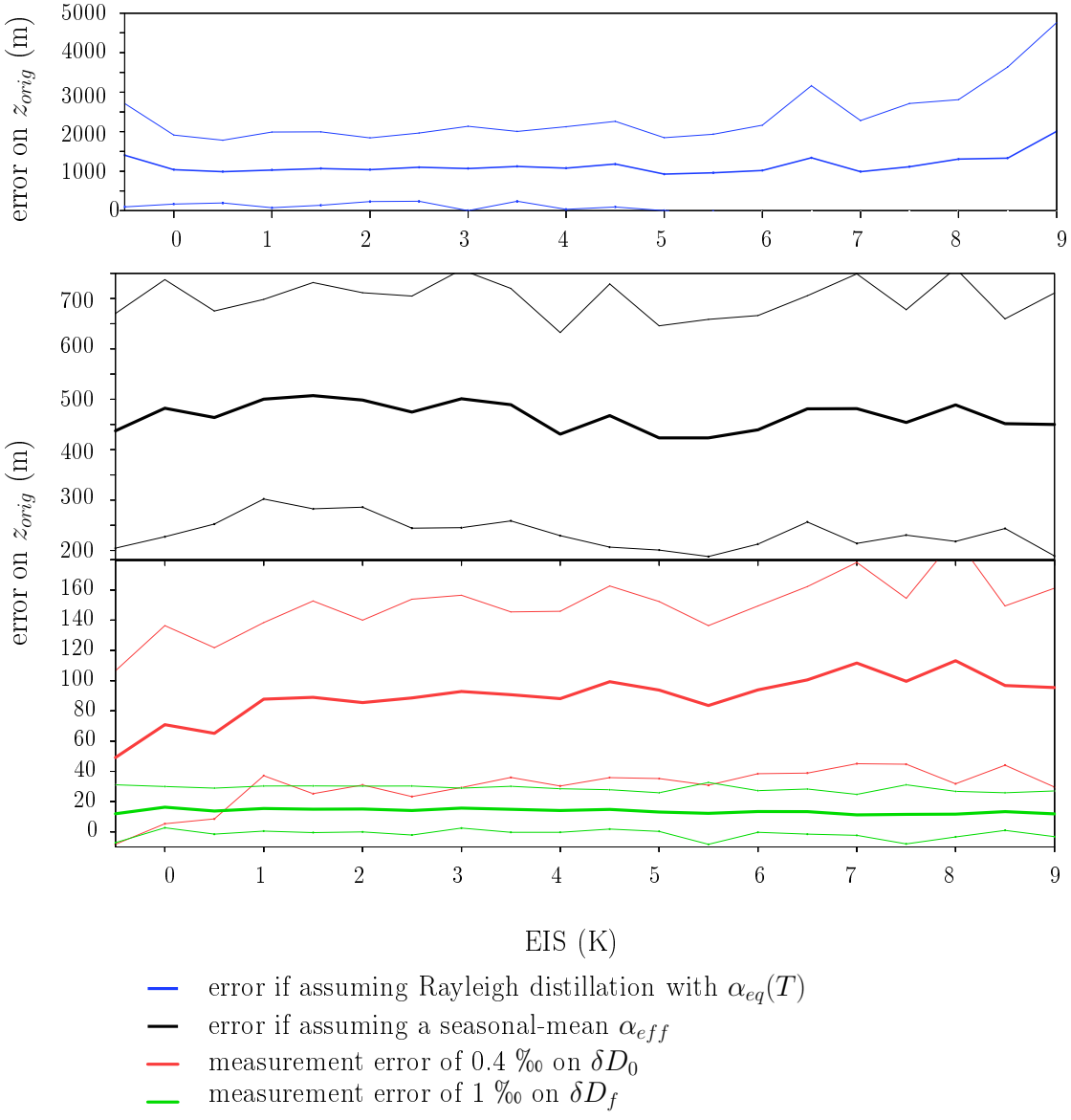

Figure 16. Errors when estimating z_{orig} from δD_0 observations, as a function of EIS, as predicted by LMDZ: error if one uses α_{eq} as a function of local temperature to estimate α_{eff} , error if one uses the seasonal-mean profile instead of the daily profile to estimate α_{eff} (black), error we would make if δD_0 is measured with a 1‰ error (red), and error we would make if δD_f is measured with a 1‰ error (green). The standard deviations among all daily errors estimated in each bin of EIS are also shown.

To summarize, δD_0 measurements could potentially be useful to estimate z_{orig} with a useful precision in cumulus and strato-cumulus clouds, but only if we are able to measure daily δD profiles and if measure δD_0 with an accuracy of 0.1 ‰ and 0.4 ‰ in trade-wind cumulus and strato-cumulus clouds respectively.

Atmos. Chem. Phys. Discuss., https://doi.org/10.5194/acp-2019-254
Manuscript under review for journal Atmos. Chem. Phys.
Discussion started: 29 March 2019

7 Conclusion

We propose an analytical model to predict the water vapor isotopic composition δD_0 of the sub-cloud layer (SCL) over tropical oceans. Benetti et al. (2015) extended the Merlivat and Jouzel (1979) closure equation to make explicit the link between δD_0 and FT entrainment. We further extend the Benetti et al. (2015) equation in two ways: first, we assume that we know the shape of the δD vertical profiles, and second, we let the altitude from which the air originates, z_{orig}, vary.

The resulting equation highlights the fact that δD_0 is not sensitive to the intensity of entrainment. Therefore, it is unlikely that water vapor isotopic measurements could help estimate the entrainment velocity that many studies have strived to estimate (Bretherton et al., 1995). In contrast, δD_0 is sensitive to the altitude from which the air originates. Based on a simulation with LMDZ and observations during the STRASSE cruise, we show that z_{orig} is an important factor explaining the seasonal-spatial and daily variations in δD_0. In turn, could δD_0 measurements, combined with vertical profiles of humidity, temperature and δD, help estimate z_{orig} and thus discriminate between different mixing processes? This should rely on a good knowledge of the δD vertical profiles. We find that for such isotope-based estimates of z_{orig} to be useful, we would need frequent vertical profiles of δD and very accurate measurements of δD_0, which are currently difficult to obtain. In precipitating clouds and deep convection, rain evaporation is too large a source of uncertainty, whereas in strato-cumulus regions, very precised estimates of z_{orig} (no larger than 20 m) would be needed to be useful. Therefore, it is in regions of shallow cumulus clouds that such isotope-based estimates of z_{orig} would be most useful.

This study is preliminary in many respects. First, it would be safe to check using water tagging experiments in LMDZ that z_{orig} estimates really represents the altitude from which the air is originates, and is not to biases by our simplifying assumptions. Second, the coarse vertical resolution of LMDZ, and the simplicity of mixing parameterizations (e.g. cloud top entrainment is not represented) are a limitation of this study. Ideally, the relationship between δD_0 , z_{orig} and the type of mixing processes should be investigated in isotope-enabled Large Eddy Simulations (LES) (Blossey et al., 2010; Moore et al., 2014). Artificial tracers and structure detection methods (Park et al., 2016; Brient et al., 2019), combined with conditional sampling methods (Couvreux et al., 2010), could help detect the different kinds of mixing structures, estimate their contributions to vertical transport, and describe their isotopic signature. This would allow us to confirm, or infirm, many of the hypotheses and conclusions in this paper. Finally, if the sensitivity of δD_0 to the type of mixing processes is confirmed, paired isotopic simulations of single-column model (SCM) versions of general circulation models (GCM) and LES, forced by the same forcing, could be very useful to help evaluate and improve the representation of mixing and entrainment processes in GCMs, as is routinely the case for non-isotopic variables (Randall et al., 2003; Hourdin et al., 2013; Zhang et al., 2013).

Code and data availability. LMDZ can be downloaded from http://lmdz.lmd.jussieu.fr/. Program codes used for the analysis are available on https://prodn.idris.fr/thredds/catalog/ipsl_public/rlmd698/article_mixing_processes/d_pgmf/catalog.html.

Isotopic measurements from STRASSE can be downloaded from http://cds-espri.ipsl.fr/isowvdataatlantic/. All other datasets and processed files are available on https://prodn.idris.fr/thredds/catalog/ipsl_public/rlmd698/article_mixing_processes/catalog.html.

Atmos. Chem. Phys. Discuss., https://doi.org/10.5194/acp-2019-254
Manuscript under review for journal Atmos. Chem. Phys.
Discussion started: 29 March 2019

Atmospheric Chemistry and Physics Discussions

Appendix A: Closure if the tropospheric profile follows a mixing line

If we assume that R_{orig} is uniquely related to q_{orig} through a mixing line between the SCL air and a dry end-member (q_f, R_f):

$$q_{orig} = a \cdot q_0 + (1-a) \cdot q_f \tag{A1}$$

and

$$R_{orig} = a \cdot q_0 \cdot R_0 + (1-a) \cdot q_f \cdot R_f \tag{A2}$$

Reorganizing Eq. (A1), we get $a = \frac{r-p}{1-p}$ with $p = q_f/q_0$. Since $q_f \leq q_{orig} \leq q_0$, $p \leq r_{orig}$. Injecting Eq. (A2) into 6, we get:

$$R_0 = \frac{R_{oce}/\alpha_{eq} + p/(1-p) \cdot R_f \cdot \alpha_K \cdot (1-h_0)}{h_0 + \alpha_K \cdot (1-h_0)/(1-p)} \tag{A3}$$

As a consistency check, in the limit case where the end-member is totally dry ($p = 0$), we find the MJ79 equation, i.e. Eq. (10).

It is intriguing to realize that r_{orig} has disappeared from Eq. (A3). This can be understood physically: if the vertical profile follows a mixing line, it does not matter at which altitude the air comes from: ultimately, what matters is how much dry air has been mixed directly or indirectly into the SCL. This can be visualize in Fig. 4b. Therefore, if R_{orig} follows a mixing line, we lose the sensitivity to z_{orig}.

Appendix B: Modification in case of rain evaporation

An important assumption that led to Eq. (9) is the neglect of SCL moistening by rain evaporation. Here we test the sensitivity to this assumption by adding a rain evaporation component. The new water vapor and isotopic budgets of the SCL write:

$$M \cdot q_{orig} + F + E = (N+D) \cdot q_0$$

$$M \cdot q_{orig} \cdot R_{orig} + F \cdot R_F + E \cdot R_E = (N+D) \cdot q_0 \cdot R_0$$

where F is the rain evaporation flux. We note $F = \eta \cdot E$. We write the isotopic composition of the rain evaporation, R_F, as:

$$R_F = \alpha_{re} \cdot R_0$$

where α_{re} is an effective fractionation coefficient. For example, if droplets are formed near the cloud base, some of them precipitate and evaporate totally in the SCL (e.g. in non-precipitating shallow cumulus clouds), then $\alpha_{re} = \alpha(T_{cloudbase})$. In

Atmos. Chem. Phys. Discuss., https://doi.org/10.5194/acp-2019-254
Manuscript under review for journal Atmos. Chem. Phys.
Discussion started: 29 March 2019

Atmospheric Chemistry and Physics Discussions

contrast, if droplets are formed in deep convective updrafts after total condensation of the SCL vapor, and then a very small fraction of the rain is evaporated in a very dry SCL, then $\alpha_{re} = 1/\alpha(T_{SCL})/\alpha_K$ (Stewart, 1975).

Combining all equations, in the case of a logarithmic δD profile, we get:

$$R_0 = \frac{R_{oce}}{\alpha_{eq}} \cdot \frac{1}{h_0 + \alpha_K \cdot (1-h_0) \cdot \frac{1-r_{orig}^{\alpha_{eff}}}{1-r_{orig}} + \eta \cdot \alpha_K \cdot (1-h_0) \cdot (1-\alpha_{re})} \tag{B1}$$

Rain evaporation can have a depleting or enriching effect depending on the sign of $1-\alpha_{re}$ (Fig. 3 pink, blue). In the paper, we thus well neglect rain evaporation effects, to avoid dealing with such an unknown parameter as α_{re}.

Author contributions. CR thought about the equations, ran the LMDZ simulations, made the analysis and wrote the manuscript. JG initiated the discussion on the subject and discussed regularly about the results. GR provided the STRASSE radiosoundings. FB provided insight and references about cloud processes. JG, GR and FB all gave comments on the manuscript.

Competing interests. The authors declare that they have no conflict of interest.

Acknowledgements. This work was granted access to the HPC resources of IDRIS under the allocation 2092 made by GENCI. We thank Marion Benetti for her previous studies on this subject and useful discussions. We thank Sandrine Bony for stimulating discussions.

References

Aggarwal, P. K., Romatschke, U., Araguas-Araguas, L., Belachew, D., Longstaffe, F. J., Berg, P., Schumacher, C., and Funk, A.: Proportions of convective and stratiform precipitation revealed in water isotope ratios, Nature Geoscience, 9, 624, 2016.

Albrecht, B. A.: Effects of precipitation on the thermodynamic structure of the trade wind boundary layer, Journal of Geophysical Research: Atmospheres, 98, 7327–7337, 1993.

Bailey, A., Toohey, D., and Noone, D.: Characterizing moisture exchange between the Hawaiian convective boundary layer and free troposphere using stable isotopes in water, Journal of Geophysical Research: Atmospheres, 118, 8208–8221, 2013.

Benetti, M., Reverdin, G., Pierre, C., Merlivat, L., Risi, C., and Vimeux., F.: Deuterium excess in marine water vapor: Dependency on relative humidity and surface wind speed during evaporation, J. Geophys. Res, 119, 584–593, DOI: 10.1002/2013JD020 535, 2014.

Benetti, M., Aloisi, G., Reverdin, G., Risi, C., and Sèze, G.: Importance of boundary layer mixing for the isotopic composition of surface vapor over the subtropical North Atlantic Ocean, Journal of Geophysical Research: Atmospheres, 120, 2190–2209, 2015.

Benetti, M., Reverdin, G., Aloisi, G., and Sveinbjörnsdóttir, Á.: Stable isotopes in surface waters of the A tlantic O cean: Indicators of ocean-atmosphere water fluxes and oceanic mixing processes, Journal of Geophysical Research: Oceans, 122, 4723–4742, 2017a.

Benetti, M., Steen-Larsen, H. C., Reverdin, G., Sveinbjörnsdóttir, Á. E., Aloisi, G., Berkelhammer, M. B., Bourlès, B., Bourras, D., De Coetlogon, G., Cosgrove, A., et al.: Stable isotopes in the atmospheric marine boundary layer water vapour over the Atlantic Ocean, 2012–2015, Scientific data, 4, 160 128, 2017b.

Betts, A. K. and Ridgway, W.: Climatic equilibrium of the atmospheric convective boundary layer over a tropical ocean, Journal of the Atmospheric Sciences, 46, 2621–2641, 1989.

Blossey, P. N., Kuang, Z., and Romps, D. M.: Isotopic composition of water in the tropical tropopause layer in cloud-resolving simulations of an idealized tropical circulation, J. Geophys. Res., 115, D24 309, doi:10.1029/2010JD014 554, 2010.

Bolot, M., Legras, B., and Moyer, E. J.: Modelling and interpreting the isotopic composition of water vapour in convective updrafts, Atmospheric Chemistry and Physics, 13(16), 7903–7935, 2013.

Bony, S., Dufresne, J.-L., Le Treut, H., Morcrette, J.-J., and Senior, C.: On dynamic and thermodynamic components of cloud changes, Climate Dynamics, 22, 71–86, https://doi.org/10.1007/s00382-003-0369-6, 2004.

Bony, S., Risi, C., and Vimeux, F.: Influence of convective processes on the isotopic composition (deltaO18 and deltaD) of precipitation and water vapor in the Tropics. Part 1: Radiative-convective equilibrium and TOGA-COARE simulations, J. Geophys. Res., 113, D19 305, doi:10.1029/2008JD009 942, 2008.

Bony, S., Stevens, B., Ament, F., Bigorre, S., Chazette, P., Crewell, S., Delanoë, J., Emanuel, K., Farrell, D., Flamant, C., et al.: EUREC4A: a field campaign to elucidate the couplings between clouds, convection and circulation, Surveys in Geophysics, pp. 1–40, 2017.

Bretherton, C. S.: Insights into low-latitude cloud feedbacks from high-resolution models, Phil. Trans. R. Soc. A, 373, 20140 415, 2015.

Bretherton, C. S., Austin, P., and Siems, S. T.: Cloudiness and marine boundary layer dynamics in the ASTEX Lagrangian experiments. Part II: Cloudiness, drizzle, surface fluxes, and entrainment, Journal of the atmospheric sciences, 52, 2724–2735, 1995.

Brient, F., Couvreux, F., Najda, V., Rio, C., and Honnert, R.: Object-oriented identification of coherent structures in large-eddy simulations: importance of downdrafts in stratocumulus, Geophy. Res. Lett., 2019.

Ciais, P., White, W., Jouzel, J., and Petit, J.: The origin of present-day Antarctic precipitation from surface snow deuterium excess data, J. Geophys. Res., 100, 18 917–18 927, 1995.

Couvreux, F., Hourdin, F., and Rio, C.: Resolved versus parametrized boundary-layer plumes. Part I: A parametrization-oriented conditional sampling in large-eddy simulations, Boundary-layer meteorology, 134, 441–458, 2010.

Craig, H. and Gordon, L. I.: Deuterium and oxygen-18 variations in the ocean and marine atmosphere, Stable Isotope in Oceanographic Studies and Paleotemperatures, Laboratorio di Geologia Nucleate, Pisa, Italy, 9–130, 1965.

Dansgaard: Stable isotopes in precipitation, Tellus, 16, 436–468, 1964.

Davini, P., D?Andrea, F., Park, S.-B., and Gentine, P.: Coherent Structures in Large-Eddy Simulations of a Nonprecipitating Stratocumulus-Topped Boundary Layer, Journal of the Atmospheric Sciences, 74, 4117–4137, 2017.

De Roode, S. R., Sandu, I., Van Der Dussen, J. J., Ackerman, A. S., Blossey, P., Jarecka, D., Lock, A., Siebesma, A. P., and Stevens, B.: Large-eddy simulations of EUCLIPSE–GASS Lagrangian stratocumulus-to-cumulus transitions: Mean state, turbulence, and decoupling, Journal of the Atmospheric Sciences, 73, 2485–2508, 2016.

De Rooy, W. C., Bechtold, P., Fröhlich, K., Hohenegger, C., Jonker, H., Mironov, D., Siebesma, A. P., Teixeira, J., and Yano, J.-I.: Entrainment and detrainment in cumulus convection: An overview, Quarterly Journal of the Royal Meteorological Society, 139, 1–19, 2013.

Dee, S. G., Nusbaumer, J., Bailey, A., Russell, J. M., Lee, J.-E., Konecky, B., Buenning, N. H., and Noone, D. C.: Tracking the Strength of the Walker Circulation With Stable Isotopes in Water Vapor, Journal of Geophysical Research: Atmospheres, 123, 7254–7270, 2018.

Delaygue, G., Masson, V., Jouzel, J., Koster, R. D., and Healy, R. J.: The origin of Antarctic precipitation: A modelling approach, Tellus, 52B, 19–36, 2000.

Dufresne, J.-L., Foujols, M.-A., Denvil, S., Caubel, A., Marti, O., Aumont, O., alkanski, Y., Bekki, S., Bellenger, H., Benshila, R., Bony, S., Bopp, L., Braconnot, P., Brockmann, P., Cadule, P., Cheruy, F., Codron, F., Cozic, A., Cugnet, D., de Noblet, N., Duvel, J.-P., Ethé, C., Fairhead, L., Fichefet, T., Flavoni, S., Friedlingstein, P., Grandpeix, J.-Y., Guez, L., Guilyardi, E., Hauglustaine, D., Hourdin, F., Idelkadi, A., Ghattas, J., Joussaume, S., Kageyama, M., Krinner, G., Labetoulle, S., Lahellec, A., Lefebvre, M.-P., Lefevre, F., Levy, C., Li, Z. X., Lloyd, J., Lott, F., Madec, G., Mancip, M., Marchand, M., Masson, S., Meurdesoif, Y., Mignot, J., Musat, I., Parouty, S., Polcher, J., Rio, C., Schulz, M., Swingedouw, D., Szopa, S., Talandier, C., Terray, P., and Viovy, N.: Climate change projections using the IPSL-CM5 Earth System Model: from CMIP3 to CMIP5, Clim. Dyn, 40 (9-10), 1–43, DOI 10.1007/s00 382–012–1636–1, 2012.

Ehhalt, D. H.: Vertical profiles of HTO, HDO, and H2O in the troposphere, NCAR technical note, NCAR-TN-STR-100, 1974.

Ehhalt, D. H., Rohrer, F., and Fried, A.: Vertical profiles of HDO/H2O in the troposphere, J. Geophy. Res., 110, D13, 2005.

Emanuel, K., Neelin, D., and Bretherton, C.: On large-scale circulations in convecting atmospheres, Quaterly Journal of the Royal Meteorological Society, 120, 1111–1143, 1994.

Ent, R. J. and Savenije, H. H.: Oceanic sources of continental precipitation and the correlation with sea surface temperature, Water Resources Research, 49(7), 3993–4004, 2013.

Faloona, I., Lenschow, D. H., Campos, T., Stevens, B., Van Zanten, M., Blomquist, B., Thornton, D., Bandy, A., and Gerber, H.: Observations of entrainment in eastern Pacific marine stratocumulus using three conserved scalars, Journal of the atmospheric sciences, 62, 3268–3285, 2005.

Field, R. D., Jones, D. B. A., and Brown, D. P.: The effects of post-condensation exchange on the isotopic composition of water in the atmosphere, J. Geophy. Res., 115, D24305, doi:10.1029/2010JD014 334, 2010.

Galewsky, J.: Using Stable Isotopes in Water Vapor to Diagnose Relationships Between Lower-Tropospheric Stability, Mixing, and Low-Cloud Cover Near the Island of Hawaii, Geophysical Research Letters, 45, 297–305, 2018a.

Galewsky, J.: Relationships between inversion strength, lower-tropospheric moistening, and low-cloud fraction in the subtropical Southeast Pacific derived from stable isotopologues of water vapor, Geophysical Research Letters, 45, 7701–7710, 2018b.

Galewsky, J. and Rabanus, D.: A stochastic model for diagnosing subtropical humidity dynamics with stable isotopologues of water vapor, Journal of the Atmospheric Sciences, 73, 1741–1753, 2016.

Galewsky, J. and Samuels-Crow, K.: Water vapor isotopic composition of a stratospheric air intrusion: Measurements from the Chajnantor Plateau, Chile, Journal of Geophysical Research: Atmospheres, 119, 9679–9691, 2014.

Galewsky, J., Strong, M., , and Sharp, Z. D.: Measurements of water vapor D/H ratios from Mauna Kea, Hawaii, and implications for subtropical humidity dynamics, Geophy. Res. Lett., 34, L22 808, doi:10.1029/2007GL031 330, 2007.

Galewsky, J., Steen-Larsen, H. C., Field, R. D., Worden, J., Risi, C., and Schneider, M.: Stable isotopes in atmospheric water vapor and applications to the hydrologic cycle, Reviews of Geophysics, 54, 809–865, 2016.

Gates, W. L.: AMIP: The Atmospheric Model Intercomparison Project, Bull. Am. Meteor. Soc., 73, 1962–1970, 1992.

Gerber, H., Frick, G., Malinowski, S., Brenguier, J., and Burnet, F.: Holes and entrainment in stratocumulus, Journal of the atmospheric sciences, 62, 443–459, 2005.

Gerber, H., Frick, G., Malinowski, S. P., Jonsson, H., Khelif, D., and Krueger, S. K.: Entrainment rates and microphysics in POST stratocumulus, Journal of Geophysical Research: Atmospheres, 118, 12–094, 2013.

Gimeno, L., A., Drumond, R., Nieto, Trigo, R. M., and Stohl, A.: On the origin of continental precipitation, Geophys. Res. Lett., 37, L13 804, doi:10.1029/2010GL043 712., 2010.

Glenn, I. B. and Krueger, S. K.: Downdrafts in the near cloud environment of deep convective updrafts, Journal of Advances in Modeling Earth Systems, 6, 1–8, 2014.

Good, S. P., Noone, D., Kurita, N., Benetti, M., and Bowen, G. J.: D/H isotope ratios in the global hydrologic cycle, Geophysical Research Letters, 42, 5042–5050, 2015.

Guilpart, E., Vimeux, F., Evan, S., Brioude, J., Metzger, J.-M., Barthe, C., Risi, C., and Cattani, O.: The isotopic composition of near-surface water vapor at the Maïdo observatory (Reunion Island, southwestern Indian Ocean) documents the controls of the humidity of the subtropical troposphere, Journal of Geophysical Research: Atmospheres, 122, 9628–9650, 2017.

Heus, T. and Jonker, H. J.: Subsiding shells around shallow cumulus clouds, Journal of the Atmospheric Sciences, 65, 1003–1018, 2008.

Heus, T., Pols, C. F. J., Jonker, H. J., Van den Akker, H. E., and Lenschow, D. H.: Observational validation of the compensating mass flux through the shell around cumulus clouds, Quarterly Journal of the Royal Meteorological Society, 135, 101–112, 2009.

Hourdin, F., Musat, I., Bony, S., Braconnot, P., Codron, F., Dufresne, J.-L., Fairhead, L., Filiberti, M.-A., Friedlingstein, P., Grandpeix, J.-Y., Krinner, G., Levan, P., Li, Z.-X., and Lott, F.: The LMDZ4 general circulation model: climate performance and sensitivity to parametrized physics with emphasis on tropical convection, Clim. Dyn., 27, 787–813, https://doi.org/10.1007/s00382-006-0158-0, 2006.

Hourdin, F., Grandpeix, J.-Y., Rio, C., Bony, S., Jam, A., Cheruy, F., Rochetin, N., Fairhead, L., Idelkadi, A., Musat, I., et al.: LMDZ5B: the atmospheric component of the IPSL climate model with revisited parameterizations for clouds and convection, Climate Dynamics, 40, 2193–2222, 2013.

Jonas, P.: Observations of cumulus cloud entrainment, Atmospheric research, 25, 105–127, 1990.

Jouzel, J. and Koster, R. D.: A reconsideration of the initial conditions used for stable water isotope models, J. Geophys. Res., 101, 22 933–22 938, https://doi.org/10.1029/96JD02362, 1996.

Khalsa, S. J. S.: Direct sampling of entrainment events in a marine stratocumulus layer, Journal of the atmospheric sciences, 50, 1734–1750, 1993.

Kurita, N.: Water isotopic variability in response to mesoscale convective system over the tropical ocean., Journal of Geophysical Research, 118(18), 10–376, 2013.

Lacour, J.-L., Risi, C., Clarisse, L., Bony, S., Hurtmans, D., Clerbaux, C., and Coheur, P.-F.: Mid-tropospheric deltaD observations from IASI/MetOp at high spatial and temporal resolution, Atmos. Chem. Phys., 12, 10 817–10 832, doi:10.5194/acp–12–10 817–2012, 2012.

Lacour, J.-L., Clarisse, L., Worden, J., Schneider, M., Barthlott, S., Hase, F., Risi, C., Clerbaux, C., Hurtmans, D., and Coheur, P.-F.: Cross-validation of IASI/MetOp derived tropospheric ?D with TES and ground-based FTIR observations, Atmospheric Measurement Techniques, 8, 1447–1466, https://doi.org/10.5194/amt-8-1447-2015, http://www.atmos-meas-tech.net/8/1447/2015/, 2015.

Lacour, J.-L., Risi, C., Worden, J., Clerbaux, C., and Coheur, P.-F.: Isotopic signature of convection's depth in water vapor as seen from IASI and TES D observations, Earth Planet. Sci. Lett., 7, 9645–9663, doi.org/10.5194/acp–17–9645–2017, 2017.

Lawrence, J. R., Gedzelman, S. D., Gamache, J., and Black, M.: Stable isotope ratios: Hurricane Olivia, J. Atmos. Chem, 41, 67–82, 2002.

Lawrence, J. R., Gedzelman, S. D., Dexheimer, D., Cho, H.-K., Carrie, G. D., Gasparini, R., Anderson, C. R., Bowman, K. P., and Biggerstaff, M. I.: Stable isotopic composition of water vapor in the tropics, J. Geophys. Res., 109, D06 115, doi:10.1029/2003JD004 046, https://doi.org/10.1029/2003JD004046, 2004.

Lee, J.-E., Pierrehumbert, R., Swann, A., and Lintner, B. R.: Sensitivity of stable water isotopic values to convective parameterization schemes, Geophy. Res. Lett., 36, doi:10.1029/2009GL040 880, 2009.

Lozar, A. and Mellado, J. P.: Evaporative cooling amplification of the entrainment velocity in radiatively driven stratocumulus, Geophysical Research Letters, 42, 7223–7229, 2015.

Majoube, M.: Fractionnement en Oxygène 18 et en Deutérium entre l'eau et sa vapeur, Journal de Chimie Physique, 10, 1423–1436, 1971.

Mellado, J. P.: Cloud-top entrainment in stratocumulus clouds, Annual Review of Fluid Mechanics, 49, 145–169, 2017.

Merlivat, L. and Jouzel, J.: Global climatic interpretation of the Deuterium-Oxygen 18 relationship for precipitation, J. Geophys. Res., 84, 5029–5332, 1979.

Moore, M., Kuang, Z., and Blossey, P. N.: A moisture budget perspective of the amount effect, Geophys. Res. Lett., 41, 1329–1335, doi:10.1002/2013GL058 302., 2014.

Moyer, E. J., Irion, F. W., Yung, Y. L., and Gunson, M. R.: ATMOS stratospheric deuterated water and implications for troposphere-stratosphere transport, Geophys. Res. Lett., 23, 2385–2388, https://doi.org/10.1029/96GL01489, 1996.

Neggers, R., Stevens, B., and Neelin, J. D.: A simple equilibrium model for shallow-cumulus-topped mixed layers, Theoretical and Computational Fluid Dynamics, 20, 305–322, 2006.

Nicholls, S. and Turton, J.: An observational study of the structure of stratiform cloud sheets: Part II. Entrainment, Quarterly Journal of the Royal Meteorological Society, 112, 461–480, 1986.

Oueslati, B., Bony, S., Risi, C., and Dufresne, J.-L.: Interpreting the inter-model spread in regional precipitation projections in the tropics: role of surface evaporation and cloud radiative effects, Climate Dynamics, pp. 1–15, 2016.

Park, S.-B., Gentine, P., Schneider, K., and Farge, M.: Coherent structures in the boundary and cloud layers: Role of updrafts, subsiding shells, and environmental subsidence, Journal of the Atmospheric Sciences, 73, 1789–1814, 2016.

Randall, D., Krueger, S., Bretherton, C., Curry, J., Duynkerke, P., Moncrieff, M., Ryan, B., Starr, D., Miller, M., Rossow, W., et al.: Confronting models with data: The GEWEX cloud systems study, Bulletin of the American Meteorological Society, 84, 455–469, 2003.

Risi, C., Bony, S., and Vimeux, F.: Influence of convective processes on the isotopic composition (O18 and D) of precipitation and water vapor in the Tropics: Part 2: Physical interpretation of the amount effect, J. Geophys. Res., 113, D19 306, doi:10.1029/2008JD009 943, 2008.

Risi, C., Bony, S., Vimeux, F., Chong, M., and Descroix, L.: Evolution of the water stable isotopic composition of the rain sampled along Sahelian squall lines, Quart. J. Roy. Meteor. Soc., 136 (S1), 227 – 242, 2010a.

Risi, C., Bony, S., Vimeux, F., Frankenberg, C., and Noone, D.: Understanding the Sahelian water budget through the isotopic composition of water vapor and precipitation, J. Geophys. Res, 115, D24110, doi:10.1029/2010JD014 690, 2010b.

Risi, C., Bony, S., Vimeux, F., and Jouzel, J.: Water stable isotopes in the LMDZ4 General Circulation Model: model evaluation for present day and past climates and applications to climatic interpretation of tropical isotopic records, J. Geophys. Res., 115, D12118, doi:10.1029/2009JD013 255, 2010c.

Risi, C., Landais, A., Bony, S., Masson-Delmotte, V., Jouzel, J., and Vimeux, F.: Understanding the 17O-excess glacial-interglacial variations in Vostok precipitation, J. Geophys. Res, 115, D10112, doi:10.1029/2008JD011 535, 2010d.

Risi, C., Noone, D., Worden, J., Frankenberg, C., Stiller, G., Kiefer, M., Funke, B., Walker, K., Bernath, P., Schneider, M., Wunch, D., Sherlock, V., Deutscher, N., Griffith, D., Wernberg, P., Bony, S., Jeonghoon Lee, D. B., Uemura, R., and Sturm, C.: Process-evaluation of tropical and subtropical tropospheric humidity simulated by general circulation models using water vapor isotopic observations. Part 1: model-data intercomparison, J. Geophy. Res., 117, D05 303, 2012a.

Risi, C., Noone, D., Worden, J., Frankenberg, C., Stiller, G., Kiefer, M., Funke, B., Walker, K., Bernath, P., Schneider, M., Wunch, D., Sherlock, V., Deutscher, N., Griffith, D., Wernberg, P., Bony, S., Lee, J., Brown, D., Uemura, R., and Sturm, C.: Process-evaluation of tropical and subtropical tropospheric humidity simulated by general circulation models using water vapor isotopic observations. Part 2: an isotopic diagnostic of the mid and upper tropospheric moist bias, J. Geophy. Res., 117, D05 304, 2012b.

Risi, C., Noone, D., Frankenberg, C., and Worden, J.: Role of continental recycling in intraseasonal variations of continental moisture as deduced from model simulations and water vapor isotopic measurements, Water Resour. Res., 49, 4136–4156, doi: 10.1002/wrcr.20 312, 2013.

Rodts, S. M., Duynkerke, P. G., and Jonker, H. J.: Size distributions and dynamical properties of shallow cumulus clouds from aircraft observations and satellite data, Journal of the atmospheric sciences, 60, 1895–1912, 2003.

Salati, E., Dall'Olio, A., Matsui, E., and Gat, J.: Recycling of water in the Amazon basin: An isotopic study, Water Resources Research, 15, 1250–1258, 1979.

Sherwood, S., Bony, S., and Dufresne, J.-L.: Spread in model climate sensitivity traced to atmospheric convective mixing, Nature, 505, 37–42, doi:10.1038/nature12 829, 2014.

Sherwood, S. C.: Maintenance of the free tropospheric tropical water vapor distribution. part II: simulation of large-scale advection, J. Clim., 11, 2919–2934, 1996.

Sodemann, H., Aemisegger, F., Pfahl, S., Bitter, M., Corsmeier, U., Feuerle, T., Graf, P., Hankers, R., Hsiao, G., Schulz, H., et al.: The stable isotopic composition of water vapour above Corsica during the HyMeX SOP1 campaign: insight into vertical mixing processes from lower-tropospheric survey flights, Atmospheric Chemistry and Physics, 17, 6125–6151, 2017.

Stevens, B.: Bulk boundary-layer concepts for simplified models of tropical dynamics, Theoretical and Computational Fluid Dynamics, 20, 279–304, 2006.

Stewart, M. K.: Stable isotope fractionation due to evaporation and isotopic exchange of falling waterdrops: Applications to atmospheric processes and evaporation of lakes, J. Geophys. Res., 80, 1133–1146, 1975.

Taylor, K. E., Stouffer, R. J., and Meehl, G. A.: An overview of CMIP5 and the experiment design, Bulletin of the American Meteorological Society, 93(4), 485–498, 2012.

Thayer-Calder, K. and Randall, D.: A numerical investigation of boundary layer quasi-equilibrium, Geophysical Research Letters, 42, 550–556, 2015.

Tremoy, G., Vimeux, F., Soumana, S., Souley, I., Risi, C., Cattani, O., Favreau, G., and Oi, M.: Clustering mesoscale convective systems with laser-based water vapor delta18O monitoring in Niamey (Niger), J. Geophys. Res., 119(9), 5079–5103, DOI: 10.1002/2013JD020 968, 2014.

Uppala, S., Kallberg, P., Simmons, A., Andrae, U., da Costa Bechtold, V., Fiorino, M., Gibson, J., Haseler, J., Hernandez, A., Kelly, G., Li, X., Onogi, K., Saarinen, S., Sokka, N., Allan, R., Andersson, E., Arpe, K., Balmaseda, M., Beljaars, A., van de Berg, L., Bidlot, J., Bormann, N., Caires, S., Chevallier, F., Dethof, A., Dragosavac, M., Fisher, M., Fuentes, M., Hagemann, S., Holm, E., Hoskins, B., Isaksen, L., Janssen, P., Jenne, R., McNally, A., Mahfouf, J.-F., Morcrette, J.-J., Rayner, N., Saunders, R., Simon, P., Sterl, A., Trenberth, K., Untch, A., Vasiljevic, D., Viterbo, P., and Woollen, J.: The ERA-40 re-analysis, Quart. J. Roy. Meteor. Soc., 131, 2961–3012, 2005.

Vial, J., Bony, S., Dufresne, J.-L., and Roehrig, R.: Coupling between lower-tropospheric convective mixing and low-level clouds: Physical mechanisms and dependence on convection scheme, Journal of Advances in Modeling Earth Systems, 8, 1892–1911, 2016.

Wang, Q. and Albrecht, B. A.: Observations of cloud-top entrainment in marine stratocumulus clouds, Journal of the atmospheric sciences, 51, 1530–1547, 1994.

Webster, C. R. and Heymsfield, A. J.: Water Isotope Ratios D/H, 18O/16O, 17O/16O in and out of Clouds Map Dehydration Pathways, Science, 302, 1742–1746, https://doi.org/10.1126/science.1089496, 2003.

Wood, R.: Stratocumulus clouds, Monthly Weather Review, 140, 2373–2423, 2012.

Wood, R. and Bretherton, C. S.: Boundary layer depth, entrainment, and decoupling in the cloud-capped subtropical and tropical marine boundary layer, Journal of climate, 17, 3576–3588, 2004.

Wood, R. and Bretherton, C. S.: On the relationship between stratiform low cloud cover and lower-tropospheric stability, Journal of climate, 19, 6425–6432, 2006.

Worden, J., Noone, D., and Bowman, K.: Importance of rain evaporation and continental convection in the tropical water cycle, Nature, 445, 528–532, 2007.

Zhang, M., Bretherton, C. S., Blossey, P. N., Austin, P. H., Bacmeister, J. T., Bony, S., Brient, F., Cheedela, S. K., Cheng, A., Del Genio, A. D., et al.: CGILS: Results from the first phase of an international project to understand the physical mechanisms of low cloud feedbacks in single column models, Journal of Advances in Modeling Earth Systems, 5, 826–842, 2013.

Zipser, E.: Mesoscale and convective scale downdrafts as distinct components of squall-line structure, Mon. Wea. Rev., 105, 1568–1589, 1977.